LBL-5791
c.1

THE EFFECT OF HEAT TREATMENTS ON THE MECHANICAL PROPERTIES OF CuNiFe SPINODAL ALLOYS

Kenneth George Kubarych
(M. S. thesis)

December 1976

Prepared for the U. S. Energy Research and Development Administration under Contract W-7405-ENG-48

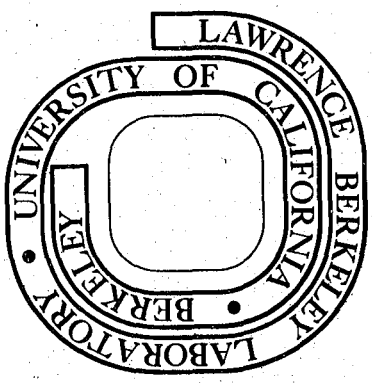

LBL-5791
c.1

THE EFFECT OF HEAT TREATMENTS ON THE MECHANICAL PROPERTIES OF CuNiFe SPINODAL ALLOYS

Contents

	ABSTRACT	iv
I.	INTRODUCTION	1
II.	EXPERIMENTAL PROCEDURE	9
III.	EXPERIMENTAL RESULTS	14
IV.	DISCUSSION	19
V.	CONCLUSIONS	28
	ACKNOWLEDGEMENTS	29
	REFERENCES	30
	TABLES	32
	FIGURE CAPTIONS	36
	FIGURES	42

THE EFFECT OF HEAT TREATMENTS ON THE MECHANICAL PROPERTIES OF CuNiFe SPINODAL ALLOYS

Kenneth George Kubarych

Materials and Molecular Research Division, Lawrence Berkeley Laboratory and Department of Materials Science and Engineering, University of California, Berkeley, California 94720

ABSTRACT

Non-conventional heat treatments were designed to produce spinodal microstructures in two CuNiFe alloys for the improvement of mechanical properties with a reduction in total aging time. The microstructures were characterized by measuring the Curie temperature to determine the composition of the NiFe rich phase and by TEM to measure the spinodal wavelength. In most cases the material failed intergranularly. However, it was only after the longer aging times that any discontinuous grain boundary coarsening was observed. The measured yield strength of both alloys was found to be proportional to the difference in lattice parameter between the two phases and independent of wavelength and nearly independent of volume fraction. The calculated values for the yield strength using Dahlgren's theory is shown to be in complete agreement with the measured values for the yield strength.

I. INTRODUCTION

The concept of spinodal decomposition was first introduced by Gibbs in 1877. However, the majority of the theoretical understanding of the subject has come through the work of Hillert, Hilliard, and Cahn and is reviewed in papers by Cahn[1] and Hilliard[2]. Theory predicts that spinodal decomposition will produce a periodic distribution of small, coherent particles or regions of two phases uniformly distributed throughout the entire crystal. Initially the periodic distribution of composition has a sinusoidal waveform but as the separation approaches completeness the wave form develops into a square wave. Also to minimize strain energy the particles align themselves along the elastically "soft" directions.

Spinodal alloys exhibit a pronounced age hardening response when aged inside the miscibility gap[3-6]. This can be attributed to the development of a modulated microstructure. The age hardening response has been treated theoretically and three different approaches are considered.

Cahn[7] considered the forces on a dislocation induced by the modulated structure. He concluded that the interaction of the dislocation with the elastic strain field accompanying the composition modulation would produce the dominant strength contributing force. This treatment predicts that the

increase in yield strength over the undecomposed alloy has a $A^2\lambda$ dependence, where A and λ are the amplitude and wavelength of the composition modulation respectively. This approach only considers the early stages of decomposition when the linearized approximation is most valid. Unfortunately, this is not of much use since it is evident from experimental information that maximum hardening does not occur while this approximation is valid[4,5].

To consider a microstructure of coherent lamella, Dahlgren[8] extended the Mott and Nabarro treatment of spherical precipitates. He based his theory on the internal coherency strains resulting from the difference in lattice parameter of the two precipitating phases. He calculated the internal stress field for a lamellar microstructure and resolved the stresses along the slip plane in order to determine the applied stress required for passage of dislocations through the microstructure. The calculation is independent of λ and nearly independent of the volume fraction of the precipitating phases, but is directly related to the difference in lattice parameter between the two phases. If the approximation of a lamellar microstructure is to be valid the interface between the two phases must be a sharp change in composition. Since calculated yield stresses using this approach have been shown to agree with experimental information[4] this approximation may often be valid.

Cahn's approach is only useful for the early stages of decomposition when the composition profile is still sinusoidal and Dahlgren's model is only useful for microstructures when spinodal decomposition is complete so that the interface between the phases is sharp. In an attempt to develop a theory which bridges the entire range of possible microstructures, Ditchek et al[9] have proposed a lattice mismatch model of hardening. Their model is based on a calculation of the shear stresses due to misfit strains caused by motion of a dislocation on its slip plane. This predicts a dependence of the change in yield strength over that of the single phase material on the composition amplitude, the wave squaring factor, and the inverse of the wavelength. The squaring factor describes how the composition modulation develops from a sine wave profile to a square wave profile. Ditchek et al have found good agreement between theory and experiment. However, the choice of the squaring factor was somewhat arbitrary.

In order to produce a spinodal microsture as an age hardening device various techniques have been applied. The most common technique, however, has been isothermal aging[3-6]. Isothermal aging produces a modulated microstructure as previously described but in an attempt to reduce the total interfacial surface energy, coarsening also takes place.

Butler et al[4] found that the CuNiFe symmetric alloy (i.e. equal volume fraction of the separting phases) coarsened before phase separation was complete but Livak et al[5] found that the coarsening in the asymmetric alloys did not occur until separation was complete. Typical maximum increases in the yield strength are two to three times the yield strength for the single phase material. Initially the yield strength increases rapidly but levels off until a saturated value is reached when complete phase separation has occurred, as shown by the Curie temperature measurements made by Butler and Livak. Accompanied with the increase in yield strength is a decrease in total elongation and generally a brittle intergranular mode of fracture[3-6].

Thomas and Vercaemer[10] incorporated spinodal decomposition with a martensitic transformation. They chose a CuNiFe alloy where the NiFe rich phase would have a martensitic transformation below it's M_S temperature. The influence of the martensitic transformation on the microhardness (as measured by Vickers microhardness) of the alloy was determined as a function of isothermal aging times before quenching below M_s. Due to the brittleness of the material no yield strength data could be obtained. Aging inside the miscibility gap and quenching below M_s produced a rapid increase in the hardness. However, for aging times greater than three minutes a steady drop in the hardness occurred.

The drop in the microhardness is attributed to the increase in interparticle spacing. To eliminate the loss of ductility and the presence of brittle intergranular fracture Plewes[11] adopted a method of thermomechanical processing. The technique was successful in eliminating these unfavorable characteristics. However, thermomechanical processing is costly and generally not technologically attractive.

Spinodal decomposition during continuous-cooling affords a convenient method of developing a spinodal microstructure and may be of some technological importance. Huston et al[12] solved the diffusion equation for spinodal decomposition during continuous-cooling. The solution predicts that the general features of the spinodal microstructure are maintained. However, the cooling rate instead of the aging temperature determines the microstructural characteristics. It was shown that the wavelength spectrum will be broader than for isothermal aging because as the aging temperature decreases the wavelength receiving maximum amplification decreases and the distribution of wavelengths with positive amplification factors increases.

Badia et al[13] applied the technique of continuous-cooling to a series of CuNiCr alloys. It was observed that the decomposition produced a modulated microstructure which

has since been determined to be of a spinodal nature[19]. Their emphasis was placed on the room temperature strength as a function of the quenching rates employed from the annealing temperature. It was concluded that hardening during continuous-cooling from the annealing temperature occurred by rapid decomposition of the parent phase. The extent of the hardening appeared to be a strong function of the cooling rate. Rapid and intermediate cooling rates produced only partial hardening while slow cooling rates produced full hardening. The microstructure of the slow cooled material gave the appearance of the two phases of slightly differing lattice parameter.

As previously mentioned, fracture testing[14] has shown that spinodally decomposed CuNiFe alloys failed intergranularly while remaining fairly ductile. This apparent contradiction is believed to be the consequence of either a discontinuous coarsening reaction at the grain boundary or possibly solute segregation at the grain boundary. The discontinuous coarsening in CuNiFe alloys has been examined by Gronsky et al[15] and has been shown to be of special importance at grain boundaries of high misorientation.

A criterion for the loss of coherency in modulated microstructures has been developed by DeFontaine[16]. It requires that the wavelength remain under a certain critical value dependent upon the magnitude of the lattice mismatch.

Experimentally the loss of coherency of the CuNiFe symmetric alloy studied by Butler occurred at $\lambda \sim 1080\text{Å}$ aged at 625°C, at $\lambda \sim 800\text{Å}$ aged at 700°C, and at $\lambda \sim 1000\text{Å}$ aged at 775°C. This puts an upper limit on $\lambda \sim 800\text{Å}$ if the microstructure of CuNiFe alloys is to remain coherent. By maintaining a coherent microstructure and reducing aging times as much as possible discontinuous coarsening may be eliminated.

In summary, the desirable microstructural features required to effectively utilize the age hardening response of spinodal alloys are as follows: It is necessary to maintain a large difference in lattice parameter between the two separating phases, an interface that has a sharp change in composition, and a wavelength as small as possible. It is also necessary to be able to achieve these desired characteristics by a purely thermal method.

To achieve the high degree of phase separation low temperature aging is necessary (see Fig. 1). However, with low temperature aging the kinetics of transformation are slow. Rapid kinetics of phase transformation occur at high temperature aging but the degree of phase separation is small. Therefore, to take advantage of the high temperature kinetics and the low temperature phase separation the

method of continous-cooling appears to be the most promising. Initially, to reduce the complexity of characterizing the microstructure during continuous-cooling the method of step aging has been adopted. This method allows examination of the microstructure through a series of well defined isothermal aging steps. It is the intent of this research to show that by controlling the microstructure through strictly thermal means it is possible to obtain higher yield strengths than were possible by isothermal aging and with a saving in aging times required.

II. EXPERIMENTAL PROCEDURE

The alloys used in this study were prepared from 99.99% purity Cu, 99.85% purity Ni, and 99.6% purity Fe. The compositions of the two alloys as determined by wet chemical analysis, in atomic percent were:

Alloy A: 51.5%Cu, 33.5%Ni, 15%Fe

Alloy B: 32.0%Cu, 45.5%Ni, 22.5%Fe

To aid in fabrication, 0.5% by weight Mn was added to each melt to act as a deoxidizer. The ingots were vaccuum melted and chill cast in copper molds to avoid segregation. They were then sealed in evacuated quartz tubes, back filled with high purity Argon and homogenized for three days at 1050°C. The one inch diameter ingots were then hot rolled at 950°C to a thickness of 0.25 inches and subsequently cold rolled to a final thickness of 0.160 inches. From this material both tensile and hardness specimens were machined.

The step aging sequence was designed by following the age hardening response through a series of specified aging temperatures. The prodecure is illustrated in Fig. 2a for alloy A and in Fig. 2b for alloy B. Step 1 consisted of solution treating the specimens at 1050°C for 1 hour

followed by an ice brine quench. The Rockwell B hardness was measured and recorded. The specimens were then aged at 767°C (using a salt pot) for three different times and again the hardness was recorded. Figures 2a and 2b show a rapid increase in hardness followed by a leveling off to a saturation value. The choice of the final aging time at 767°C was a balance between obtaining high hardness and short aging times. In this case the optimum aging time for step 2 was estimated to be 15 min. Once the aging time for step 2 was determined all the remaining specimens were aged at this condition. The same procedure was applied at each aging temperature in order to determine the complete aging sequence. Since the age hardening response of the two alloys was quite similar the same aging sequence was used for both alloys. The entire step aging sequence is illustrated schematically in Fig. 3. As expected the high aging temperatures required short aging times and as the temperature was lowered the aging times increased.

The continuously-cooled specimens were placed in quartz tubes that were evacuated and back filled with argon. The specimens were then put in a horizontal tube furnace which was powered by a programable furnace control unit. Linear cooling rates of 25°C/hr. and 12.5°C/hr. were used

starting from a temperature of 900°C (above the miscibility gap) for a duration of 24 hours in both cases (see Fig. 4).

Mechanical properties were measured from standard flat tensile specimens with a 1" gage length, a 1/8" gage width, and a 0.100" gage thickness. Tests were performed on an Instron testing machine. Three specimens for each aging condition were tested at room temperature and all specimens were pulled at a constant rate of 0.02 cm/min. The yield strength was measured at 0.01% offset and the total elongation was measured from the change in length of the 1 inch gage length. The work hardening rate (i.e. the slope of the stress strain curve) was measured at 2% plastic strain for all specimens tested. A scanning electron microscope was used to determine the mode of fracture.

To qualitatively follow the state of decomposition the Curie temperature of the Ni-Fe rich phase was followed during the aging sequence. The equipment used to measure the Curie temperature is similar to that previously described[17]. Essentially, the specimen acts as the core of a transformer. A 3000 cps signal is applied to the primary coil which induces a magnetic field in the specimen which in turn

induces a current in the secondary coil. The voltage due to the induced current was filtered and amplified before recording it on the ordinate of an x-y plotter. The temperature of the specimen was measured by a chrom-alumel thermocouple spot welded to the specimen and recorded on the abscissa of the x-y plotter. Specimens were taken from the grip areas of the tensile specimens. A pure nickel specimen was used to calibrate and check the performance of the apparatus. The accuracy of the measurements was estimated to be less than ±7°C.

Electron microscope specimens were thinned from the grip areas of the tensile specimens. The material was thinned mechanically to 0.030" then chemically thinned in a solution of 1 part HF acid to 9 parts HNO_3 acid diluted to approximately 1/2 strength. This was followed by a light grinding on 600 grit sand paper to a thickness of ~4 mils. Discs were spark cut from the thinned sheets. Foils were prepared by jet polishing in a solution of HNO_3 acid/Methanol having a composition of 1:3. At a polishing temperature of -38°C a voltage of ~10v was required to produce a current ~35 ma. These conditions tended to yield the best results and were maintained quite closely.

The wavelength of the aged specimens was measured directly from the micrographs. All micrographs were taken in the <100> orientation with a strong 200 reflection operating. The microscope magnification was calibrated using a carbon replica of a ruled grating.

Light optical specimens were also taken from the grip areas of the tensile specimens. Polished optical specimens were swabbed with an etchant of the composition

10g. $FeCl_3$

200ml ethyl alcohol

50-95% H_2O.

The amount of dilution varied so as to maintain optimal etching conditions.

III. EXPERIMENTAL RESULTS

Tables I and II summarize the results of the experimental work. To be sure the hardness data collected during the design of the step aging treatment is reproducable the Rockwell "B" hardness of the tensile specimens was measured and the results are shown in Fig. 5. Comparing Fig. 2 with Fig. 5 one sees that the data is reproducable. The general features of the curves are the same; there is initially a rapid increase in hardness (high temperature aging) followed by a much slower increase in hardness (low temperature aging). For each alloy the hardness of the tensile specimens was slightly higher than the specimens used to design the step aging sequence, which is probably due to residual stresses left after machining the tensile specimens.

The results of the measurements of the yield strength are shown in Figs. 6a and 7a and are compared with available isothermal aging data. The symmetric alloy A is compared with Butler's[4] results and the NiFe rich alloy B is compared with Livak's[5] results. Both alloys, whether step aged or continuously-cooled, show a considerable increase in the maximum yield strength over the isothermally

aged case. The yield strength of the step aged material increases steadily as the aging temperature is lowered. The increase in yield strength results in a loss of total elongation similar to that observed with isothermal aging. The work hardening rate at 2% strain, for step aged specimens, increases as the aging temperature decreases. The work hardening rate of alloy A was always slightly higher than that found for alloy B. Also, the work hardening rate for the continuously-cooled material was much higher than either the step aged or isothermally aged material. The work hardening rate of alloy A was higher for the 25°C/hr cooling treatment while the work hardening rate of alloy B was higher for the 12.5°C/hr cooling treatment.

Fractography showed that the material failed in a completely ductile manner after step 1 (i.e., fast quenched from above the miscibility gap); but after all subsequent aging treatments, both step aging and continuous-cooling, failure occurred by a mixture of both brittle intergranular fracture and ductile fracture (see Figs. 8-11). Also, striations were often observed on the flat intergranular fracture surfaces.

Figures 6b and 7b show the variation of Curie temperature with aging time and are compared to the results of Butler and Livak for alloys A and B respectively. Table III gives the Curie temperatures corresponding to the equilibrium tie-line compositions as determined by the specific isothermal aging temperature. The Curie temperatures measured after each aging step are nearly equal to the Curie temperature of the equilibrium tie-line compositions. Also, the Curie temperature of the continuously-cooled material is equal to the Curie temperature of the equilibrium tie line composition of the phase expected at the lower range of aging temperatures.

The transmission electron micrographs, Fig. 12 and Fig. 14a, show the microstructures of alloy A after various stages in the step aging sequence and after the continuous-cooling rate of 25°C/hr. The microstructures of alloy B after both the final aging step and the end of the 25°C/hr continuous-cooling treatment are shown in Fig. 13 and Fig. 14b. In all the microstructures observed there appeared to be a well defined boundary between the two phases and the shape of the phases was either rods or plates with the interfaces parallel to the {100} planes.

All wavelengths measured were larger than 150Å. Therefore, since satellites cannot be resolved in the electron diffraction patterns, all measurements of wavelengths were made from the micrographs (e.g. Figs. 12-14). Figures 6c and 7c show the variation of wavelength with aging time for the various aging techniques used. The wavelength of alloy A increased steadily as the step aging sequence advanced. However, the rate of increase was much slower than the commonly observed $(\text{time})^{1/3}$ law[4,15]; the observed growth rate of λ was $(\text{time})^{0.07}$. For comparison, photographs of the microstructures achieved by isothermal aging are shown in Fig. 15 and Fig. 16. Figure 15 is from alloy A aged at 625°C for 200 hrs. and figure 16a is from alloy B aged at 625°C for 10 hrs. Alloy A aged at 625°C for 200 hrs. shows the interfaces between the two separating phases to be flat and parallel to the {100} planes but the interfaces when alloy B was aged at 625°C for 10 hrs. appeared to be wavy even though the particles did tend to align themselves on the {100} planes.

The structure of the grain boundaries for the material step aged for the early stages of the sequence showed no

evidence of discontinuous coarsening (Fig. 17). During the later stages of the sequence, however, the beginning of discontinuous grain boundary coarsening was observed (Fig. 13b,c). The material continuously-cooled also showed the early stages of discontinuous coarsening (Figs. 18,19).

Optical metallography suggested that some grain boundary thickening had occurred (Figs. 20, 21). However, as shown by the electron micrographs the affected area was of the order of 0.2μm which is approaching the resolution limit of optical metallography. Also shown in Figs. 20 and 21 is the presence of numerous voids approximately 2 to 3μm in diameter. Alloy B has a slightly higher density of voids than alloy A. The voids were observed throughout the entire history of the material and were products of the casting method.

IV. DISCUSSION

The yield strength was found to increase as the aging temperature decreased (Figs. 6a and 7a) which is consistent with the results of Butler[4] and Livak[5]. It was also found that the microstructure between the material step aged, continuously-cooled, or isothermally aged differ little. The morphology of the two phase mixture was virtually identical in all cases except for the wavelength (Figs. 12-16). It is apparent that at any aging temperature the maximum yield strength is limited (e.g., Figs. 7a,c, isothermal aging) by the difference in lattice parameter between the two phases. This has been shown to be true and was also found to be independent of the aging history. For example alloy A aged 200 hrs. at 625°C reached a yield strength of 49.7 ksi and also after step 5 (650°C) of the step aging sequence had a yield strength of 49.6 ksi. Even though the aging history is much different the final step aging temperature and the isothermal aging temperature are nearly the same giving similar values for the yield strength. By comparing the wavelength measurements and

the Curie temperature measurements of the step aged material with that of the isothermally aged material (Fig. 6b and Figs 6c, 12c, 15) it is noticed that wavelengths differ by almost a factor of two, yet the Curie temperatures are equal. This suggests that the yield strength is independent of the wavelength but dependent on the composition of the two phases, or more correctly the difference in lattice parameter, since the Curie temperature is a measure of the composition of the NiFe rich phase.

The importance of the low temperature aging is brought out by aging step 7 (550°C). Both alloys A and B show an increase in the yield strength over the values found after either step aging step 6 (600°C) or isothermal aging at 625°C. The increase in yield strength can be attributed to an increase in the difference in lattice parameter between the two separating phases. The age hardening response of alloy B has exactly the same characteristics as alloy A. The results of alloy B nicely show that the yield strength is independent of the aging history since the measured yield strengths after the 6th step of the step aging sequence, the continuous-cooling rate of 12.5%/hr. for 24hrs. or the isothermal aging treatment for 10 hrs. at 625°C were virtually the same for all three cases.

The change in composition of the NiFe rich phase

during the aging sequence was determined by measuring the Curie temperature after each aging step. The Curie temperature is the temperature at which a ferromagnetic material transforms into a paramagnetic material and is a function of composition. Since early stages of spinodal decomposition produce a continuously varying composition, the Curie temperature measured is actually of some average composition. This makes quantitative analysis of the compositions impossible for early stages, but facilitates the detection of the completion of "spinodal" decomposition. Because the Curie temperature measured is due to some average composition when the measured Curie temperature corresponds to the equilibrium tie-line composition, phase separation must necessarily be complete (i.e., a square wave composition distribution). Comparing the measured Curie temperature (Figs. 6b and 7b) with the Curie temperature of the equilibrium tie-line compositions at the appropriate temperatures, (Table III) it is shown that the measured Curie temperature closely follows the Curie temperature of the equilibrium composition through the entire aging sequence. The Curie

temperatures of the continuously-cooled material (Figs. 6b and 7b) are also near the Curie temperatures corresponding to the equilibrium composition. These measurements imply that the composition distribution has maintained a square wave profile which was observed in the electron micrographs (Fig. 12), since the interfaces appear to be sharp during the entire aging sequence. This means that by step aging it was possible to add to the amplitude of the composition profile with little change in the wavelength. Therefore, in the true sense of the word spinodal decomposition was complete before aging step 2 was complete.

A microstructure that is described by a square wave composition profile fits the model of a lamellar microstructure. Therefore, Dahlgren's calculation of the yield stress should be appropriate throughout the entire step aging sequence. The yield stress may be calculated using Dahlgren's theory from the equation

$$\sigma_i = 2Gf\epsilon$$

where G is the average shear modulus, ϵ is the misfit parameter between the two phases and f is the volume fraction of the precipitating phase. Following Butler's approach,

the equation for the yield stress in psi becomes

$$\sigma_i = 1.8 \times 10^6 \Delta_a .$$

This equation assumes the two phases have similar elastic constants and Poissons ratio is ~1/3 so that the misfit parameter may be written as $\varepsilon \sim 2/3$ where $\delta = \Delta a/a$ and a is the average lattice parameter. Also the values $f \sim 1/2$ (alloy A), $G \sim 9.9 \times 10^6$ psi and $a = 3.58\mathring{A}$ were used. The difference in lattice parameter between the two phases may also be approximated by $\Delta a \sim k\Delta\ \theta_i$ where k is a constant of proportionality. With the addition of this approximation the expression for the yield stress becomes

$$\sigma_i = 1.8 \times 10^6 (k\theta_c) .$$

The constant may be evaluated from the experimental information of Dahlgren and Bulter. Dahlgren measured a value of $\Delta a/a$ $0.03\mathring{A}$ when isothermally aged at 625°C and Butler measured a value of $\Delta a/a$ $0.021\mathring{A}$ when isothermally aged at 775°C. Therefore, using Dahlgren's value for $\Delta a/a$, $k_D = 1.0 \times 10^{-4}$/°C and using Butler's value for $\Delta a/a$, $k_B = 1.1 \times 10^{-4}$/°C. To help make the calculations more accurate k_D is used for low temperature aging and k_B is used for high temperature aging. A summary of the calculations is given in Table IV.

The calculated yield stress vs. $\Delta a/a$ is shown in Fig. 22. Also shown in the figure is the experimentally measured yield stress. The value of $\Delta a/a$ used in plotting the measured yield stress was the ideal value that should be achieved at the specific aging temperatures. A composite of the measured yield stresses for a variety of aging treatments vs. the measured Δa's, as determined from the Curie temperature measurements, is shown in Fig. 23. Also shown in Fig. 23 for comparison is the theoretical calculation for alloy A using Dahlgren's model. The agreement between the calculated and observed yield stresses is quite good in all cases. To a good approximation the yield stress varies linearly with Δa (Fig. 23), which gives good evidence that Dahlgren's model is appropriate in this case. Dahlgren's model also predicts that the yield strength is independent of the interparticle spacing and nearly independent of the volume fraction of the precipitating phases. It has been shown that the yield stress is independent of the wavelength. Also it is apparent that the yield strength is nearly independent of the volume fraction, since the greatest difference in yield strength between alloys A and B is only about 10% for similar aging treatments.

The morphology of the grain boundaries during the early stages of aging is completely unaffected by grain boundary coarsening (see Fig. 17). During the later stages of aging, discontinuous grain boundary coarsening is present (see Figs. 13b,c, 18, 19). However, the mode of fracture was the same whether the grain boundary coarsening was or was not present (see Figs. 8 and 9). The fracture surface pictured in Figs. 8c,d corresponds to the microstructure shown in Fig. 17 while the fracture surface pictured in Figs. 9g,h corresponds to the microstructure shown in Fig. 19. Even though the microstructures differ considerably the fracture surfaces are quite similar. In either case fracture occurred by a mixture of both brittle and ductile modes. In fact, single grains have appeared to have failed partially by a brittle mode and partially by a ductile mode.

It has been experimentally observed that specimens quenched from the single phase region failed in a completely ductile manner while specimens aged for as little as six minutes showed evidence of intergranular fracture[5]. Yet, specimens aged at high temperatures (775°C and 800°C) for times greater than 10 hours showed a reversal back to ductile fracture[18]. Also, it was observed that even in the worst cases some areas of ductile fracture were present along

with the intergranular fracture.

A very rapid change from ductile fracture to a mixture of both brittle and ductile fracture was also observed in this study. The brittle fracture appeared to be intergranular but numerous brittle fracture surfaces have wavy striations running across the surface. These striations are believed to be slip steps. Figures 10a and 11a show a partially separated grain boundary, clearly striations are present on the grain boundary surface. Other grain boundaries do not have striations but do show micro-void coalescence and dimpled rupture (see Fig. 8f,h and 9f,h). Also areas of ductile fracture are present (see Fig. 8f and 10b).

Experimentally a dependence of the yield strength on the grain size has been observed[14]. The dependence can easily be explained by dislocation pile-ups at the grain boundaries. The presence of dislocation pile-ups at the grain boundaries can explain the brittle intergranular fracture and the slip steps on the fracture surfaces. If a dislocation pile-up becomes large enough then a crack could open up and propagate along the grain boundary leaving a step on the fracture surface behind. The propagation of the crack is thought to be made possible by either discontinuous coarsening or solute segregation at the grain boundaries.

SUGGESTIONS FOR FUTURE RESEARCH

The actual mechanism for the presence of intergranular fracture is not yet understood. This is quite important and must be solved before full utilization of the spinodal microstructure can be realized. In the absence of grain boundary coarsening Auger spectroscopy may be useful in determining if a segregation problem exists at the grain boundaries. Electron microscopy of deformed specimens and experiments with an in situ deformation stage might reveal the mechanism of the grain boundary pinning. A more detailed examination of the morphology of the grain boundaries and its relation to the fracture characteristics should also be useful.

This study can also be directly extended to an in depth study of continuous-cooling. Continuous-cooling offers a practical method of controlling the microstructure which in turn controls the mechanical properties. Therefore, the mechanical properties can be optimized by careful choice of the heat treatment.

V. CONCLUSIONS

1. The yield strength, in this study, was found to be only a function of the difference in lattice parameter between the two separating phases and independent of the wavelength and nearly independent of the volume fraction.

2. During the entire step aging sequence the microstructure was a two phase mixture of nearly equilibrium tie-line composition.

3. The mechanical properties were sensitive only to the lowest aging temperature the material experienced and is independent of the aging history.

4. The experimentally measured yield strengths are in excellent agreement with the values calculated using Dahlgren's model.

5. The reduction in time to produce full hardening in alloy A is significant but little reduction in aging time was achieved in alloy B. However, the treatments are not necessarily the optimum.

ACKNOWLEDGEMENTS

The author would like to express his appreciation to Professor Gareth Thomas for his advice and encouragement during this study. He is also grateful to Masuo Okada and Ronald Gronsky for their many helpful discussions during the course of this work. For his invaluable assistance with the Curie temperature measurements he wishes to thank Dr. T. Peterson.

This work was done under the ausnices of the United States Energy Research and Development Administration through the Materials and Molecular Research Division of the Lawrence Berkeley Laboratory, Univeristy of California, Berkeley.

REFERENCES

1. Cahn, J. W., The 1967 Institute of Metals Lecture, "Spinodal Decomposition," Trans. AIME, 242,(1968), 166-180.

2. Hilliard, J. E., "Spinodal Decomposition", Phase Transformation, 1968 ASM Seminar, H. I. Aaronson, ed., ASM Metals Park Ohio.

3. Carpenter, R. W., Acta Met., 15, (1297), 1967.

4. Butler, E. P. and Thomas, G., Acta Met., 18, (347), 1970.

5. Livak, R. J. and Thomas, G., Acta Met., 19, (497), 1971.

6. Schwartz, L. H., Mahajan, S., Plewes, J. T., Acta Met., 22, (601), 1974.

7. Cahn, J. W., Acta Met., 11, (1275), 1963.

8. Dahlgren, S. D., Ph.D. Thesis, University of California, Berkeley, UCRL-16846, May, 1966.

9. Ditchek, B. and Schwartz, L. H., Private communication.

10. Thomas, G. and Vercaemer, C., Metallurgical Transactions, 3, (2501), 1972.

11. Plewes, J. T., in Proc. of the Third International Conference on the Strength of Metals and Alloys, Vol. 1, p. 109, Cambridge, England (1973).

12. Huston, E. L., Cahn, J. W., and Hilliard, J. E., Acta Met., 14, (1053), 1966.

13. Badia, F. A., Kirby, G. N., and Mihalisin, J. R., ASM Trans- Quart., 60, (395), 1967.

14. Livak, R. J. and Gerberich, W. W., in Proc. of the Fifth International Materials Symposium, U. C. Berkeley, (1971).

15. Gronsky, R. and Thomas, G., Acta Met., 23, (1163), 1975; R. Gronsky, M. S. Thesis, University of Calif., Berkeley, LBL-3134.

16. De Fontaine, D., Acta Met. 17, (477), 1969.

17. Goldberg, A., Dent. W. U., and Miller, J. H., J. Scient. Instrum., 44, (200), 1967.

18. Livak, R. J., Ph.D. Thesis, University of California, Berkeley, LBL-1107, September, 1972.

19. Wu, COK., M. S. Thesis, University of California, Berkeley, LBL-5729, December, 1976.

TABLE I Experimental Results, Alloy A: 51.5%Cu, 33.5%Ni, 15%Fe

Heat Treatment	Yield Strength ksi (MPa)	ULT ksi (MPa)	Total % Elongation	dσ/de ksi (MPa)	Curie Temperature °C	λ (Å)	Hardness R_B
Step 1	28.6 (197)	71.0 (490)	27.3	152 (1050)	233	-	60.4
Step 2	37.3 (257)	74.4 (513)	21.1	183 (1260)	413	225	66.7
Step 3	39.2 (270)	75.2 (518)	19.6	189 (1303)	478	245	79.8
Step 4	42.9 (296)	78.1 (538)	16.3	212 (1460)	484	-	81.9
Step 5	49.6 (342)	81.2 (560)	13.1	212 (1460)	494	300	85.4
Step 6	55.9 (385)	85.9 (592)	13.1	216 (1490)	514	-	89.0
Step 7	59.5 (410)	89.2 (615)	9.0	211 (1450)	521	315	92.0
Cont-Cool 901-300	64.5 (445)	98.7 (681)	12.3	466 (3210)	515	430	-
Cont-Cool 900-600	60.6 (418)	93.0 (641)	13.9	422 (2910)	507	330	-

TABLE II Experimental Results, Alloy B: 32%Cu, 45.5%Ni, 22.5%Fe

Heat Treatment	Yield Strength ksi (MPa)	UTS ksi (MPa)	Total % Elongation	dσ/dε ksi (MPa)	Curie Temperature °C	λ (Å)	Hardness R_B
Step 1	21.5 (148)	67.5 (465)	39.1	143 (986)	396	-	60.0
Step 2	31.5 (217)	70.1 (483	27.4	152 (1050)	392	-	72.7
Step 3	37.6 (259)	75.7 (522)	20.5	175 (1210)	428	-	78.7
Step 4	42.3 (292)	75.2 (518)	15.5	162 (1120)	466	-	84.4
Step 5	47.5 (328)	77.8 (536)	13.3	170 (1170)	492	-	87.2
Step 6	51.0 (352)	78.3 (540)	14.8	165 (1140)	518	-	90.6
Step 7	54.8 (378)	82.0 (565)	10.4	180 (1240)	522	365	93.2
Cont-Cool 900-300	57.9 (399)	95.5 (658)	14.5	387 (2667)	515	330	-
Cont-Cool 900-600	54.1 (373)	81.5 (562)	14.0	457 (3150)	507	440	-

TABLE III

Curie temperature of equilibrium compositions at various temperatures

Step	Temperature °C	Time	Equilibrium Curie Temperature °C	
			Alloy A	Alloy B
1	1050	2 hr	240	370
2	767	15 min	440	
3	740	20 min	465	
4	700	40 min	485	
5	650	1.5 hr	500	
6	600	3 hr	510	
7	550	5 hr	515	

TABLE IV · Calculation of Yield Strength for Alloy A

	Aging Treatment	$\Delta\theta_c$ °C	Δa Å	δ	σ_y calculated ksi (MPa)	σ_y measured ksi (MPa)
Isothermal Aging	625	265	0.030	6.0084	55.5 (383)	49.7 (343)
	775	205	0.021	0.0059	38.8 (268)	37.0 (255)
Step Aging	2	200	0.020	0.0038	37.8 (261)	37.3 (297)
	3	225	0.023	0.0064	42.6 (294)	39.2 (296)
	4	245	0.026	0.0074	48.9 (337)	42.9 (296)
	5	260	0.029	0.0082	54.4 (375)	49.6 (342)
	6	270	0.0306	0.0083	55.2 (381)	55.9 (385)
	7	275	0.031	0.0087	57.4 (396)	59.5 (410)

FIGURE CAPTIONS

Fig. 1. The pseudo-binary section along the tie-line of the Cu-Ni-Fe system used for this study showing the two alloy compositions. The chemical spinodal was calculated by Butler[4] using T_c = 825°C and C_c = 0.50.

Fig. 2. An illustration of the method used to design the step aging sequence. A series of isothermal aging experiments were performed to optimize (a balance between Rockwell B hardness and aging time) the aging conditions used at each temperature for a) alloy A, b) alloy B.

Fig. 3. A schematic representation of the entire step aging treatment.

Fig. 4. A schematic representation of the two cooling rates used for the continuous-cooling experiments. Top line represents a rate of 12.5°C/hr and the bottom line represents a 25°C/hr rate.

Fig. 5. The Rockwell B hardness of the tensile specimens followed through the step aging sequence. The top curve is for alloy A and the lower curve is for alloy B.

Fig. 6. A summary of the experimental information on Alloy A.

(a) Plot of yield stress vs. total aging time. The numbers correspond to the last aging step in the step aging sequence.

(b) Plot of Curie temperature vs. total aging time.

(c) Plot of wavelength vs. total aging time.

In each case step aging and continuous-cooling are compared to isothermal data at 625°C (taken from Ref. 4).

Fig. 7. A summary of the experimental information on Alloy B.

(a) Plot of yield stress vs. total aging time. The numbers correspond to the last aging step in the step aging sequence.

(b) Plot of Curie temperature vs. total aging time.

(c) Plot of wavelength vs. total aging time.

In each case step aging and continuous-cooling are compared to isothermal data at 625°C (taken from Ref. 5).

Fig. 8. Scanning electron fractographs of alloy A after (a,b) step 1, (c,d) step 3, (e,f) step 5, (g,h) step 7. This shows the change from ductile fracture to intergranular fracture and that areas of ductile fracture are present throughout.

Fig. 9. Scanning electron fractographs of alloy B after, (a,b) step 1, (c,d) step 3, (e,f) step 5 and (g,h) step 7. This shows the change from ductile fracture to intergranular fracture and that areas of ductile fracture are present throughout.

Fig. 10. Scanning electron micrograph of alloy A. (a) cooling rate 25°C/hr, (b) 12.5°C/hr. This shows the intergranular fracture. Also present are numerous steps on the fracture surfaces that are slip steps.

Fig. 11. Scanning electron micrograph of alloy B. (a) cooling rate 25°C/hr, (b) 12.5°C/hr. This shows the intergranular fracture. Also present are numerous steps on the fracture surfaces that are slip steps.

Fig. 12. Transmission electron micrographs of alloy A during the step aging sequence. a) after step 2, λ~225Å, b) after step 3, λ~245Å, c) after step 5, λ~300Å, and d) after step 7, λ~315Å.

Fig. 13. Electron micrographs of alloy B after step 7 of the step aging sequence, a) λ~365Å. b) shows a grain boundary unaffected by discontinuous coarsening while c) shows a coarsened boundary.

Fig. 14. Electron micrographs showing the spinodal microstructure for the material continuously-cooled at 25°C/hr, a) Alloy A, λ~430Å, b) Alloy B, λ~330Å

Fig. 15. Electron micrograph of Alloy A aged at 625°C for 200 hrs., λ~730A. (Courtesy of E. P. Butler).

Fig. 16. Electron micrograph of a) alloy B aged at 625°C for 10 hrs. λ~130Å and b) alloy A aged at 625°C for 5 hrs. λ~180Å. (Taken from Ref. 5).

Fig. 17. Transmission electron micrograph of alloy A showing the unaffected grain boundary after step 3 of the step aging sequence. This is a grain boundary typical of the early stages of the step aging sequence. Note the absence of grain boundary coarsening.

Fig. 18. Electron micrographs of alloy A continuously-cooled at a rate of 25°C/hr. a) A low magnification picture showing the presence of both coherent and discontinuously coarsened grain boundaries, b) A magnified view of a discontinuously coarsened grain boundary, and c) a magnified view of a coherent grain boundary.

Fig. 19. Electron micrographs of alloy B continuously-cooled at a rate of 25°C/hr. a) A low magnification picture showing the presence of both coherent and discontinuously coarsened grain boundaries and b) is a magnified view of a coarsened grain boundary.

Fig. 20. Optical micrograph of alloy A after (a) step 2, (b) step 5, (c) step 7. This shows the absence of discontinuous coarsening and the presence of numerous voids.

Fig. 21. Optical micrograph of alloy B after (a) step 2, (b) step 5, (c) step 7. This shows the absence of discontinuous coarsening and the

presence of numerous voids. The density of voids in alloy B is higher than that in alloy A.

Fig. 22. A comparison of the calculated yield stress with the yield stress from the step aged material vs. Δa/a. The calculation was performed using the theory developed by Dahlgren[8] and following the method of Butler[4]. The measured yield stress data is shown vs. the ideal Δa/a as determined from the equilibrium tie-line compositions at each specific aging temperature.

Fig. 23. A composite plot of the measured yield stresses vs. the measured Δa's, as determined from the Curie temperature measurements, for a variety of aging treatments. The calculated yield stresses for alloy A are also shown for comparison. The isothermal data for alloy A is taken from Ref. 4 and for alloy B from Ref. 5.

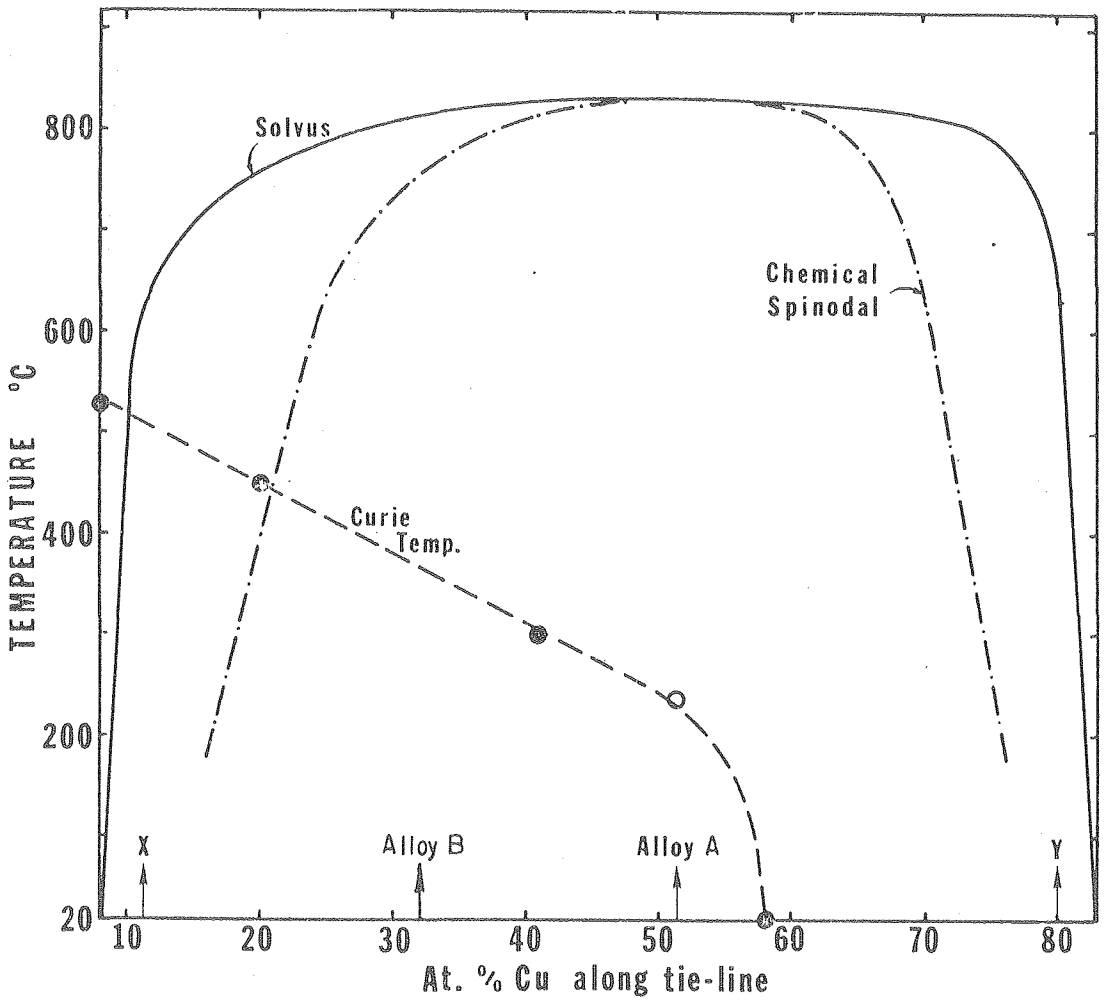

XBL 693-293A

Fig. 1

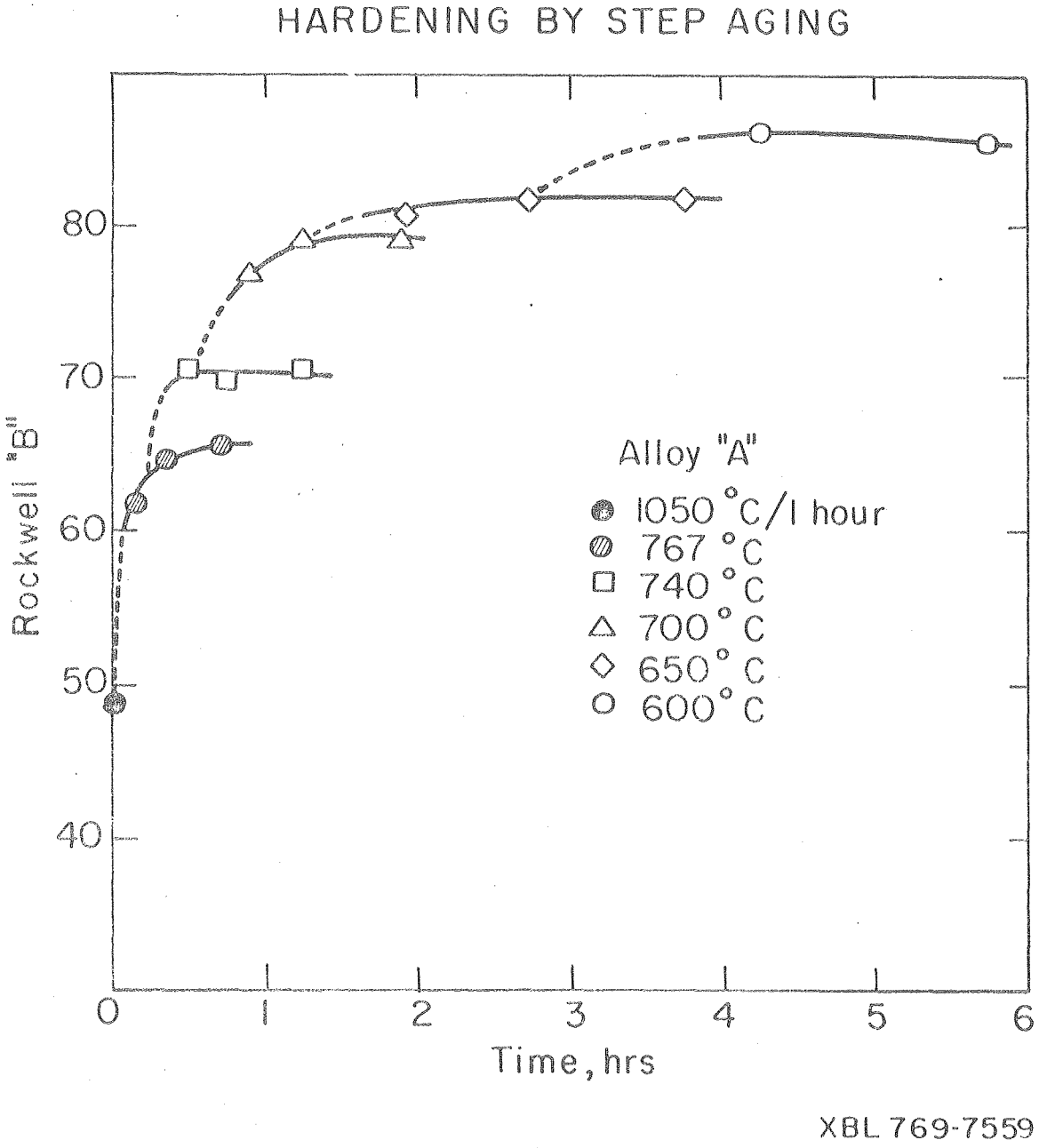

Fig. 2a

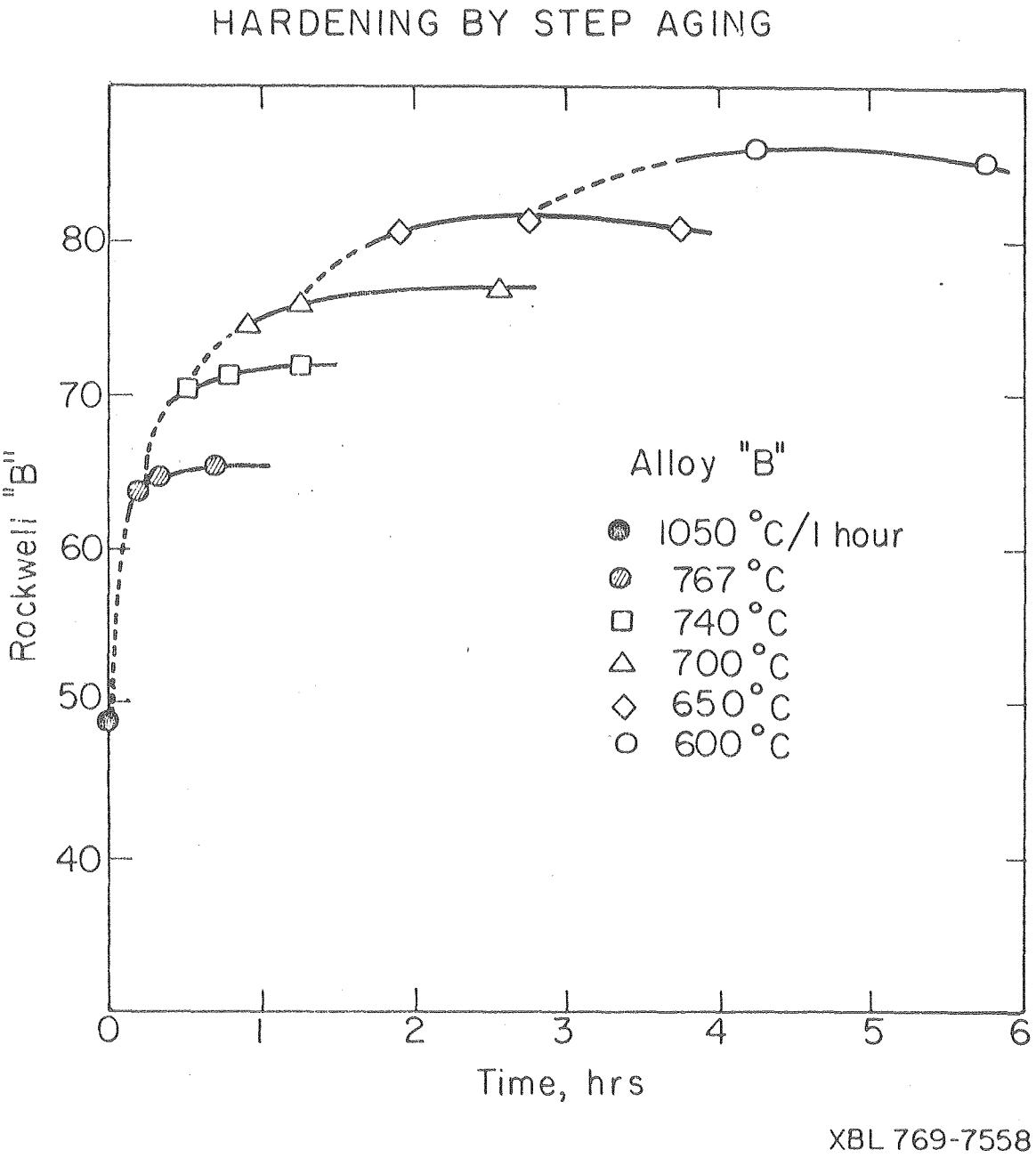
HARDENING BY STEP AGING
Rockwell "B"
80
70
60
50
40
0
1
2
3
4
5
6
Time, hrs
Alloy "B"
1050 °C/1 hour
767 °C
740 °C
700 °C
650 °C
600 °C
XBL 769-7558

Fig. 2b

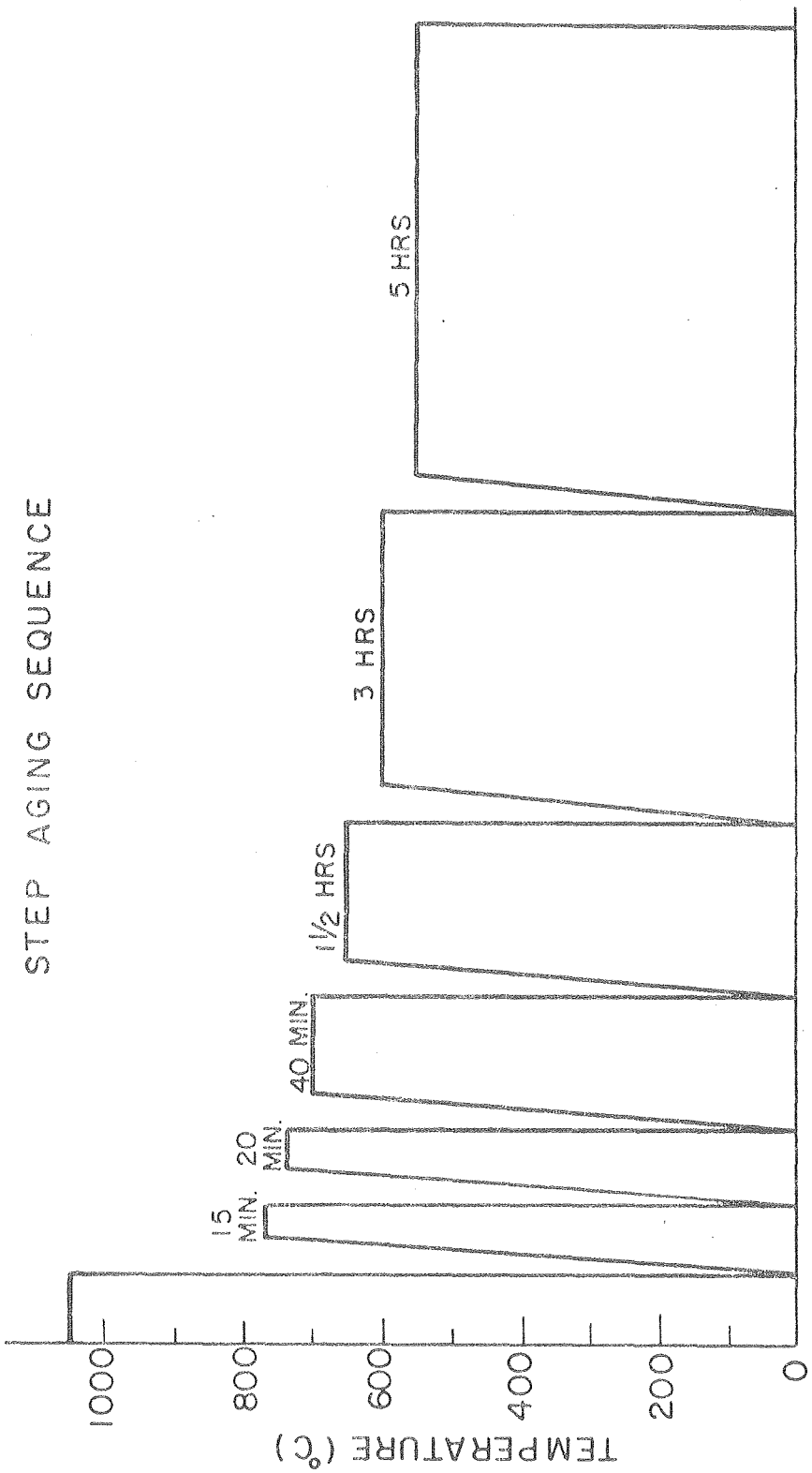
STEP AGING SEQUENCE
TEMPERATURE (°C)
1000
800
600
400
200
0
TIME
15 MIN.
20 MIN.
40 MIN.
1/2 HRS
3 HRS
5 HRS
XBL769-7524

Fig. 3

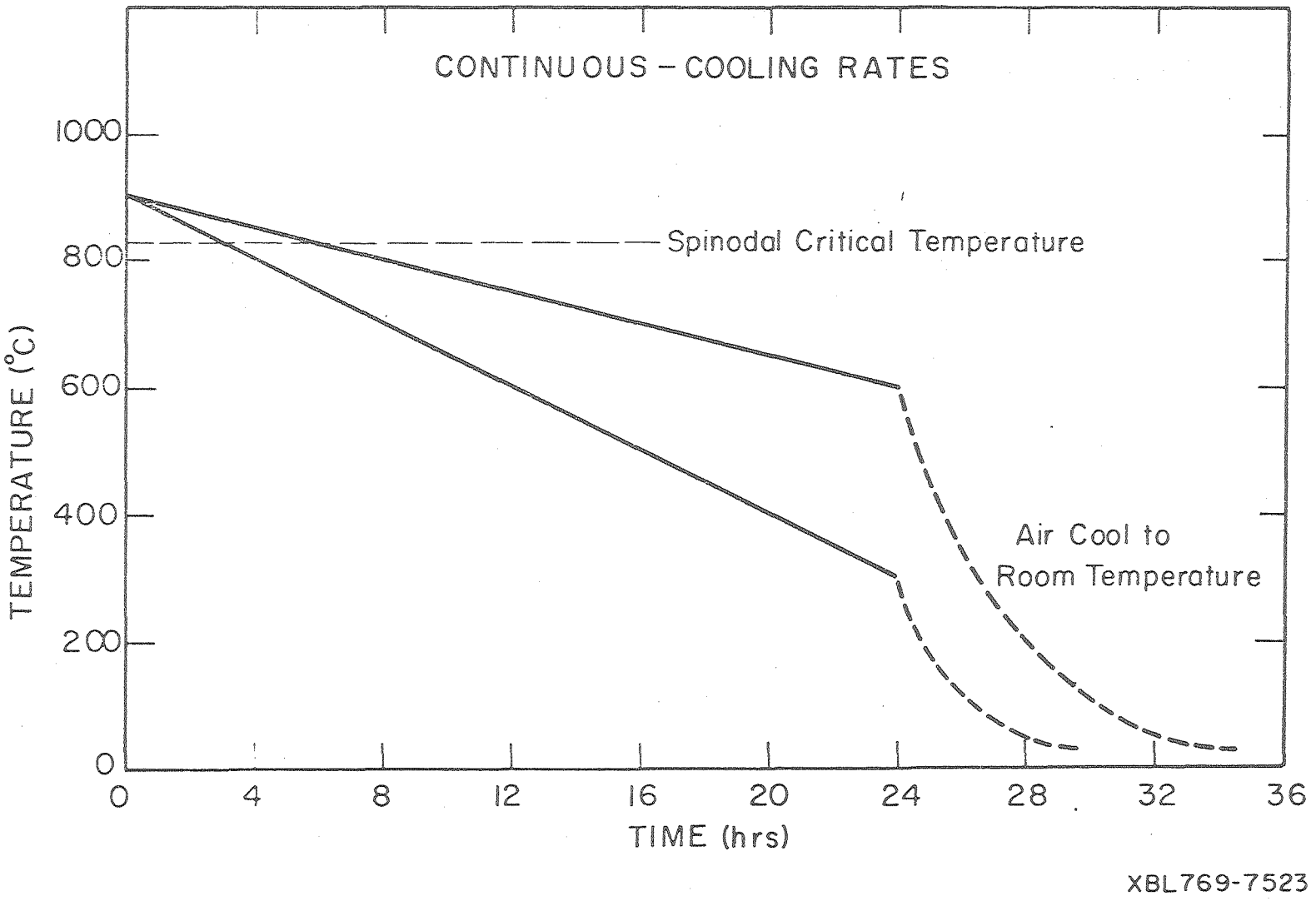
CONTINUOUS – COOLING RATES
1000
800
600
400
200
0
TEMPERATURE (°C)
Spinodal Critical Temperature
Air Cool to
Room Temperature
0
4
8
12
16
20
24
28
32
36
TIME (hrs)
XBL769-7523

Fig. 4

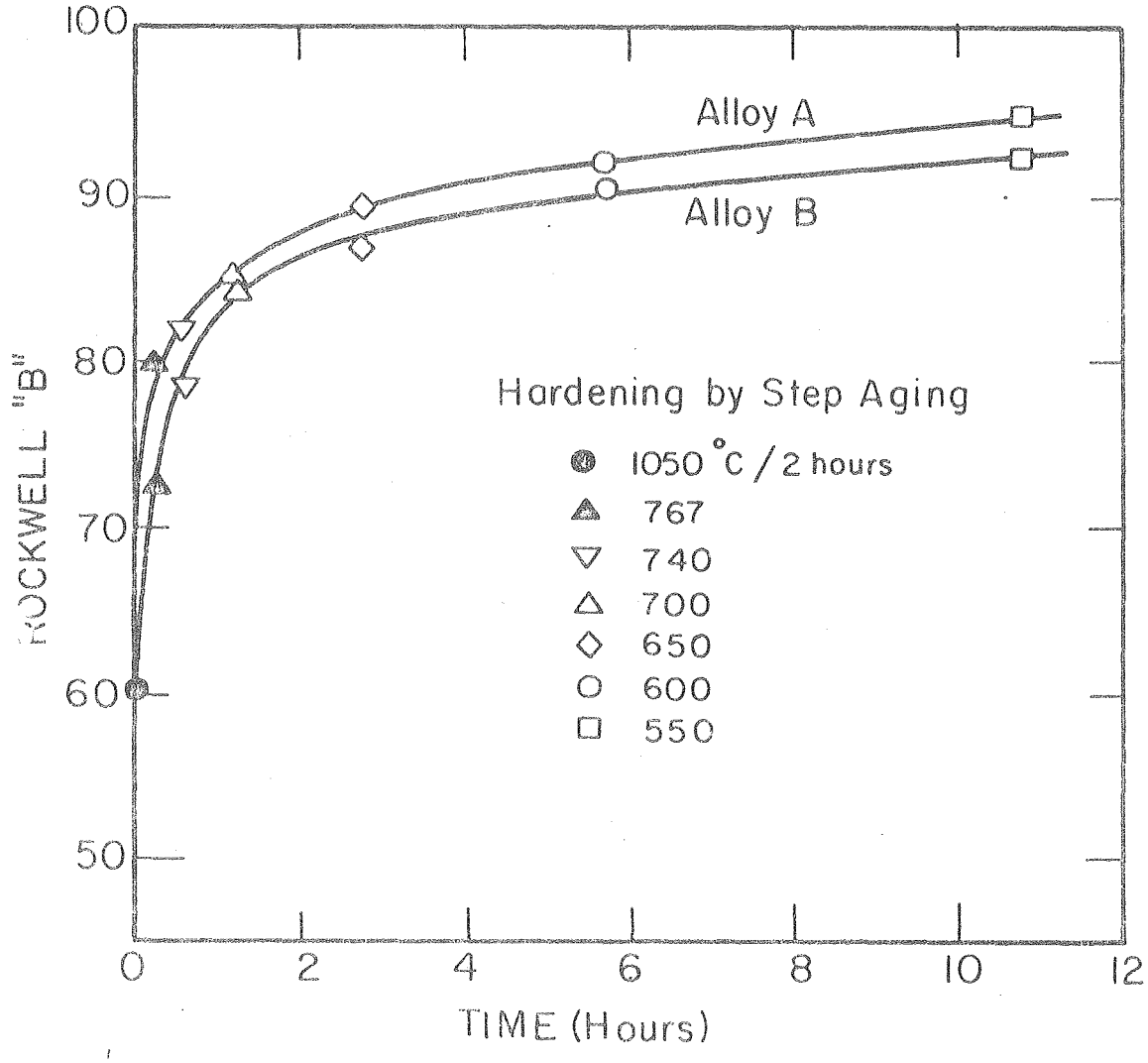

XBL 7611-7814

Fig. 5

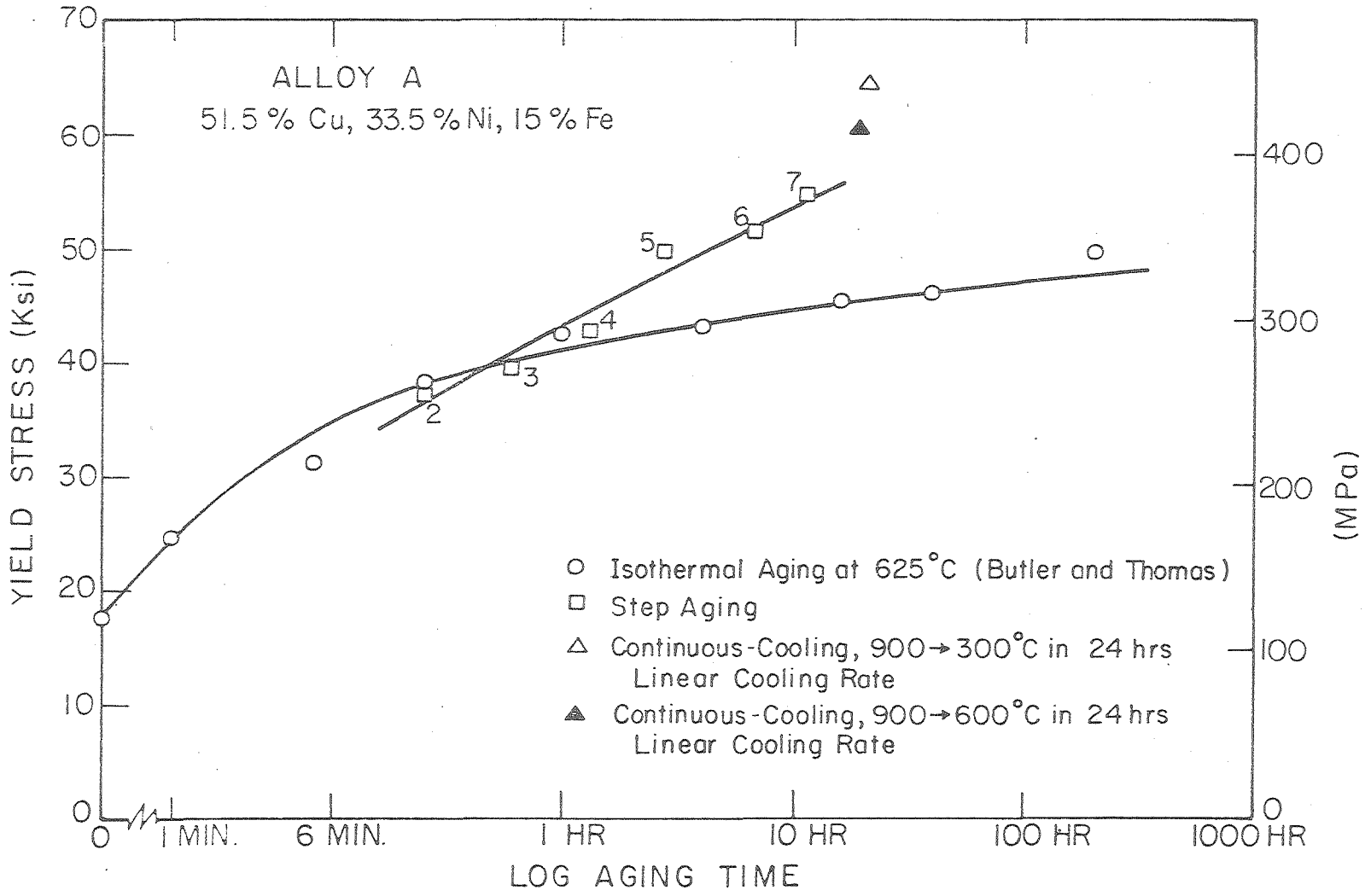

XBL 769-7525

Fig. 6a

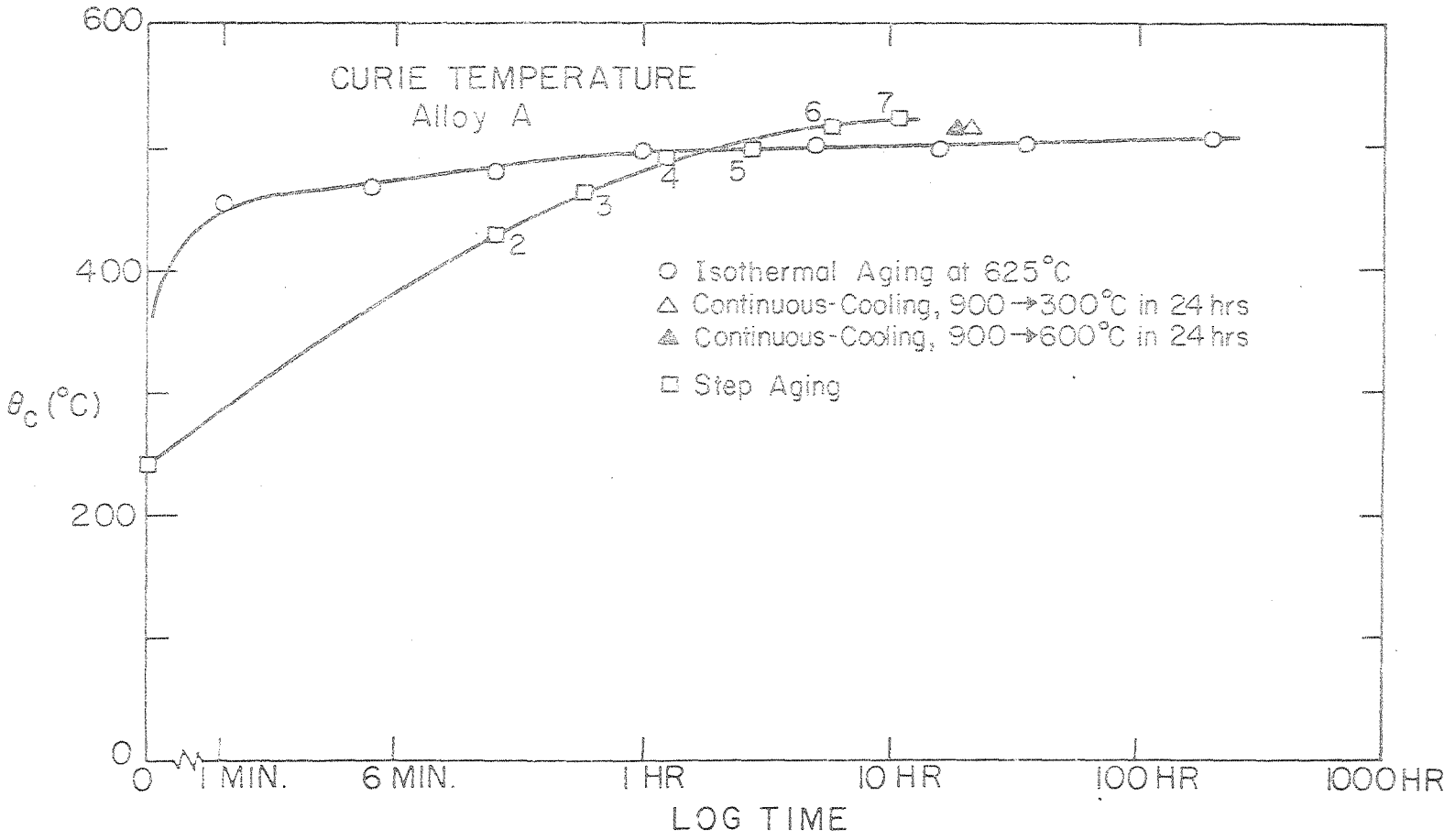

Fig. 6b

XBL 769-7540A

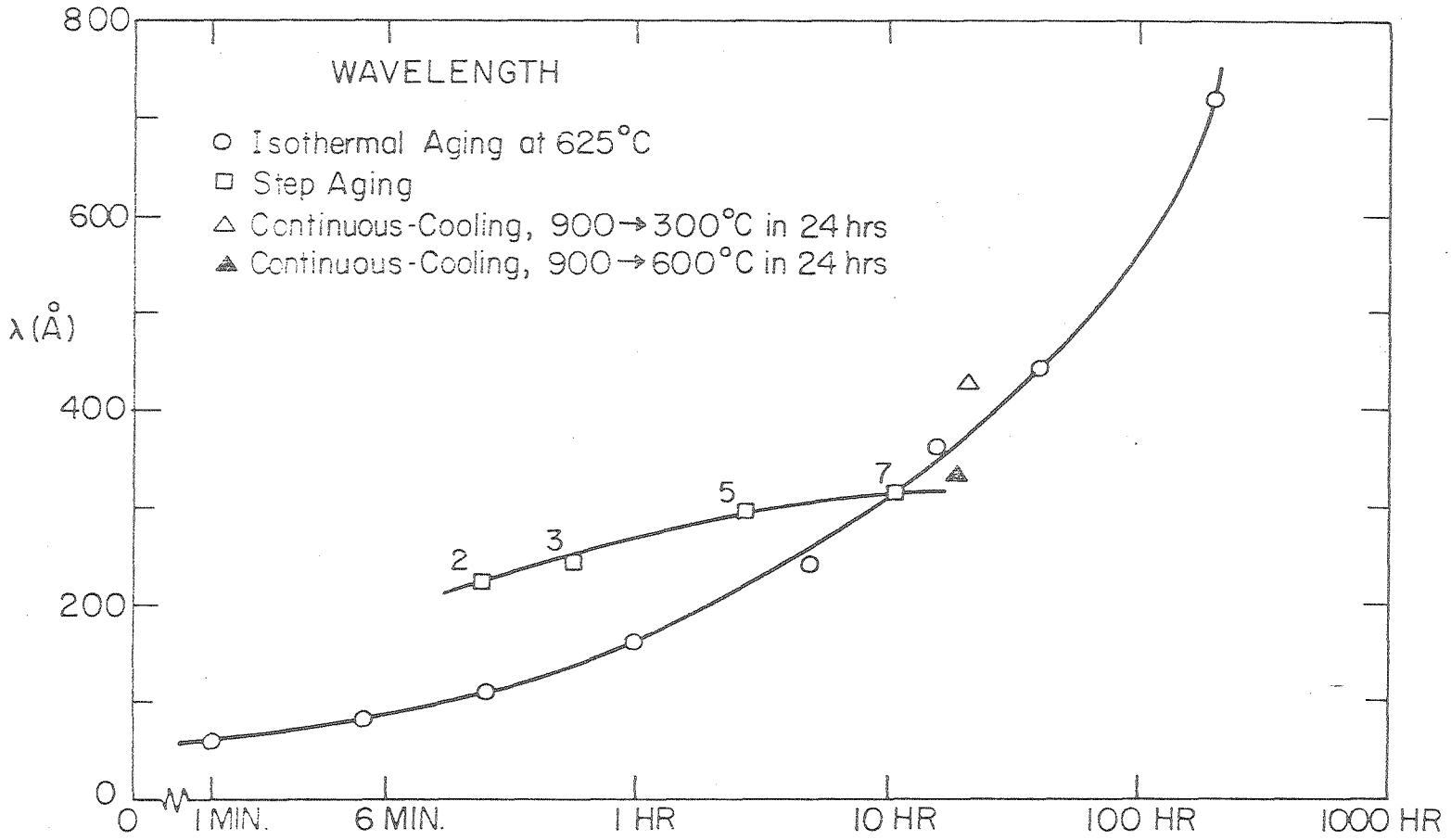

Fig. 6c

XBL 769-7539

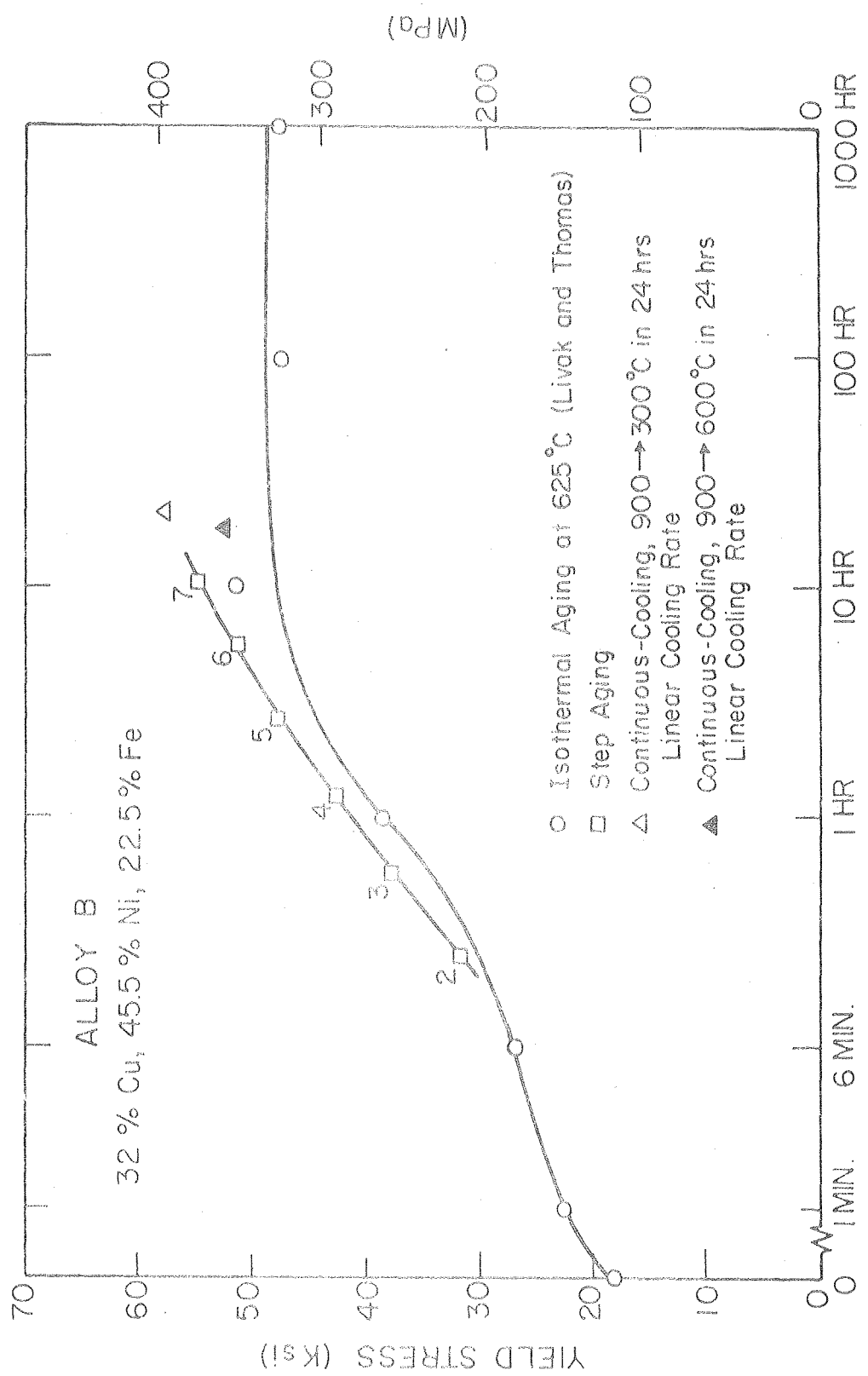

XBL 769-7526

Fig. 7a

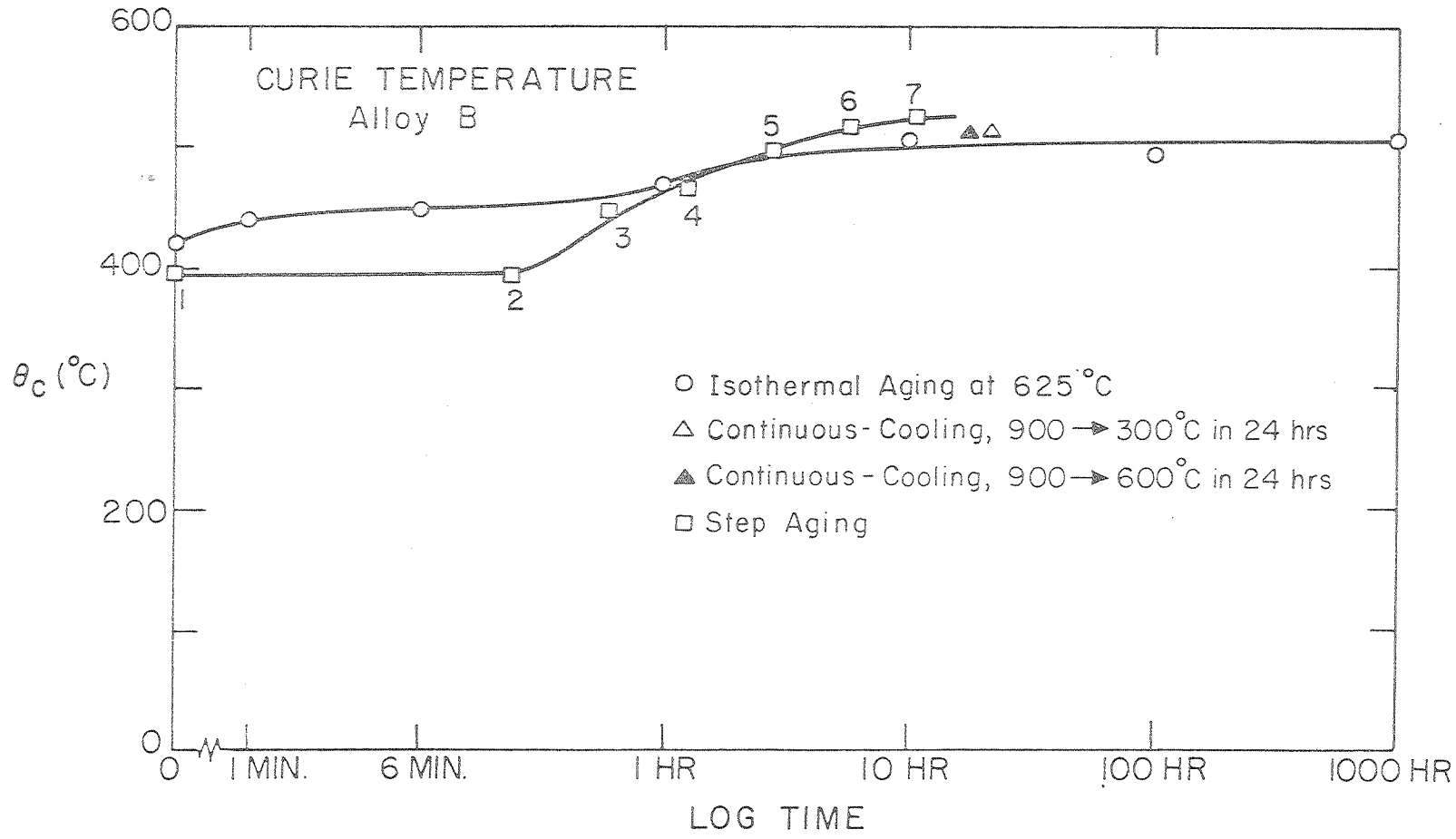

Fig. 7b

XBL 7611-7777

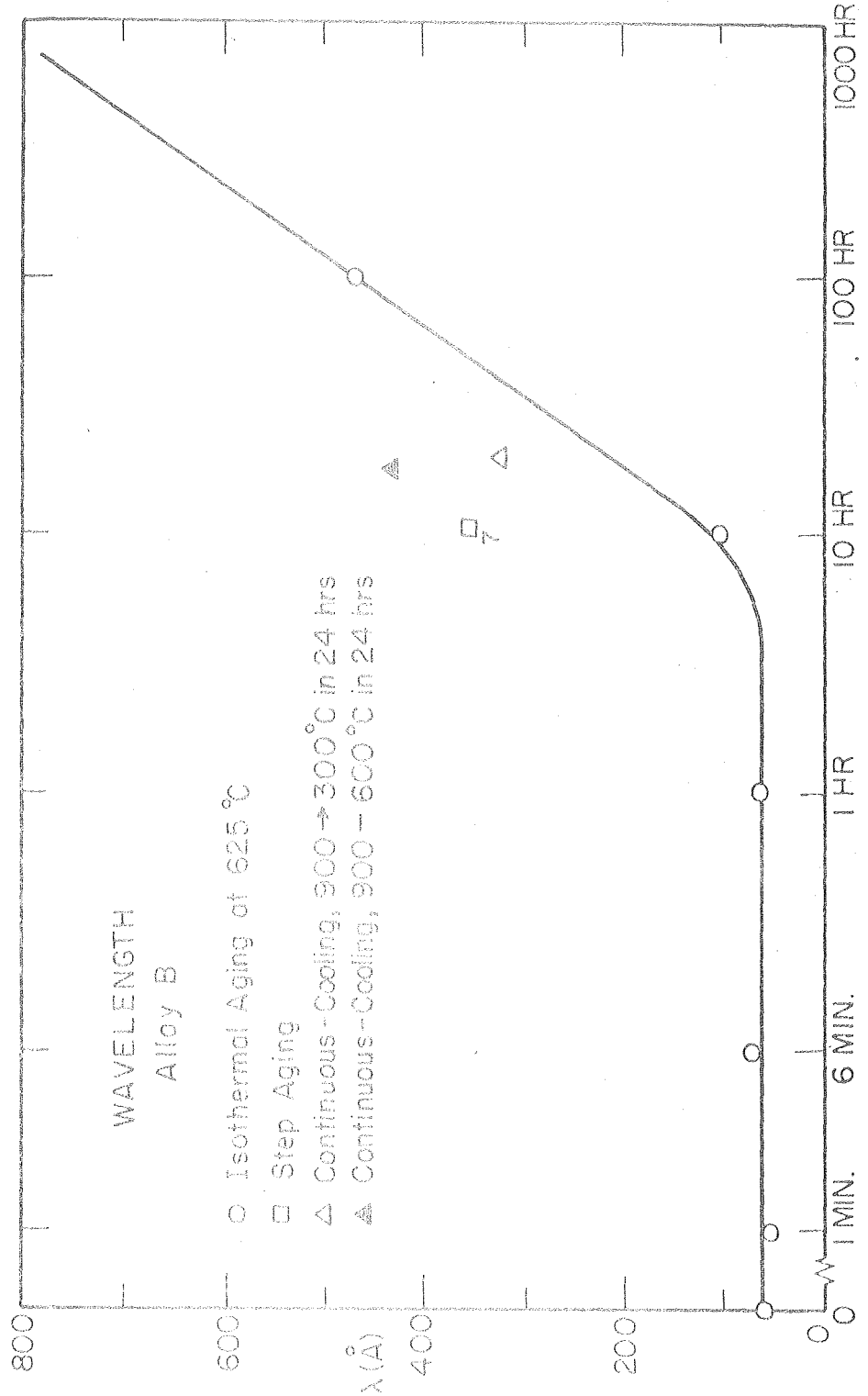

XBL 7611-7779

Fig. 7c

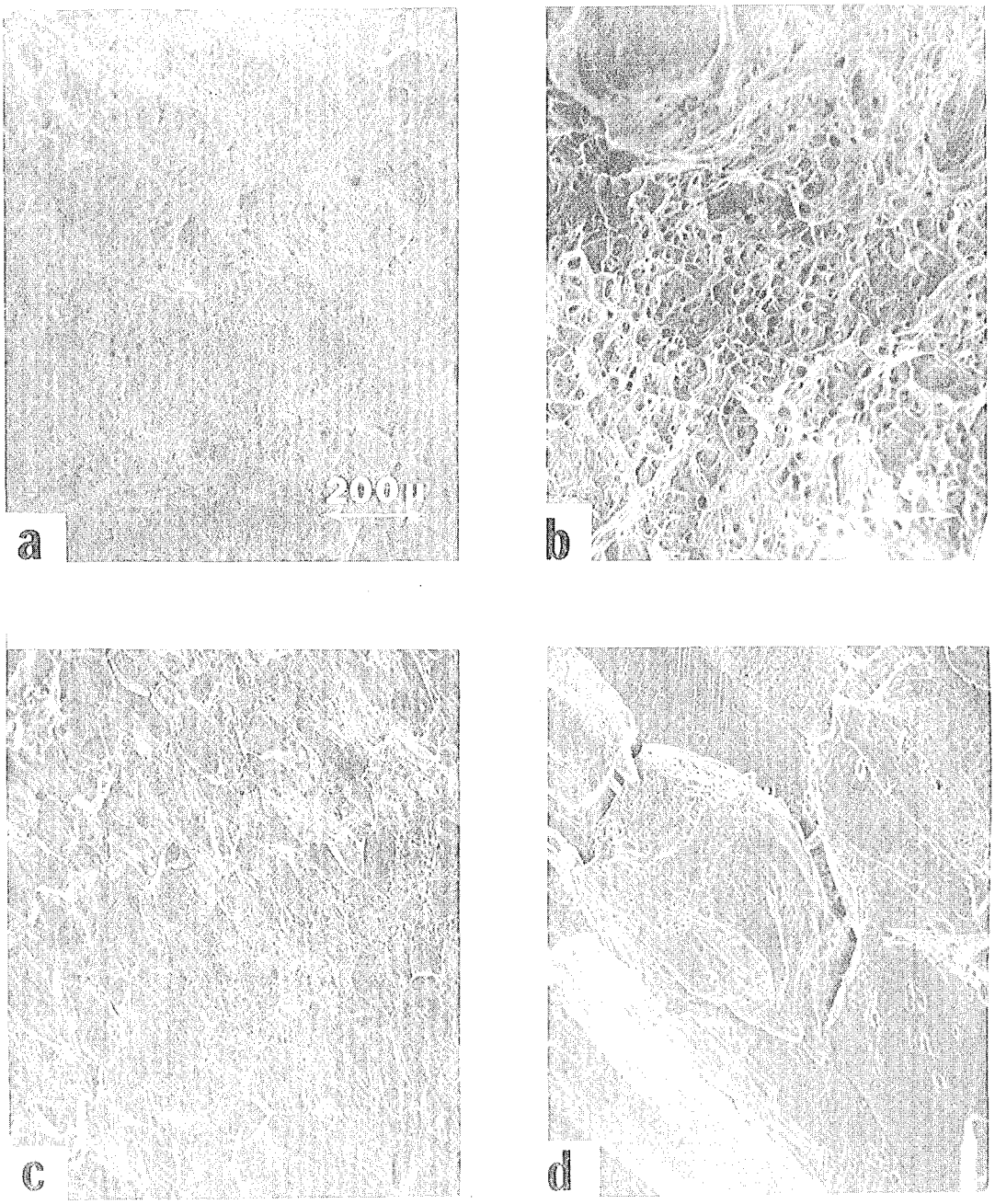

Fig. 8a-d

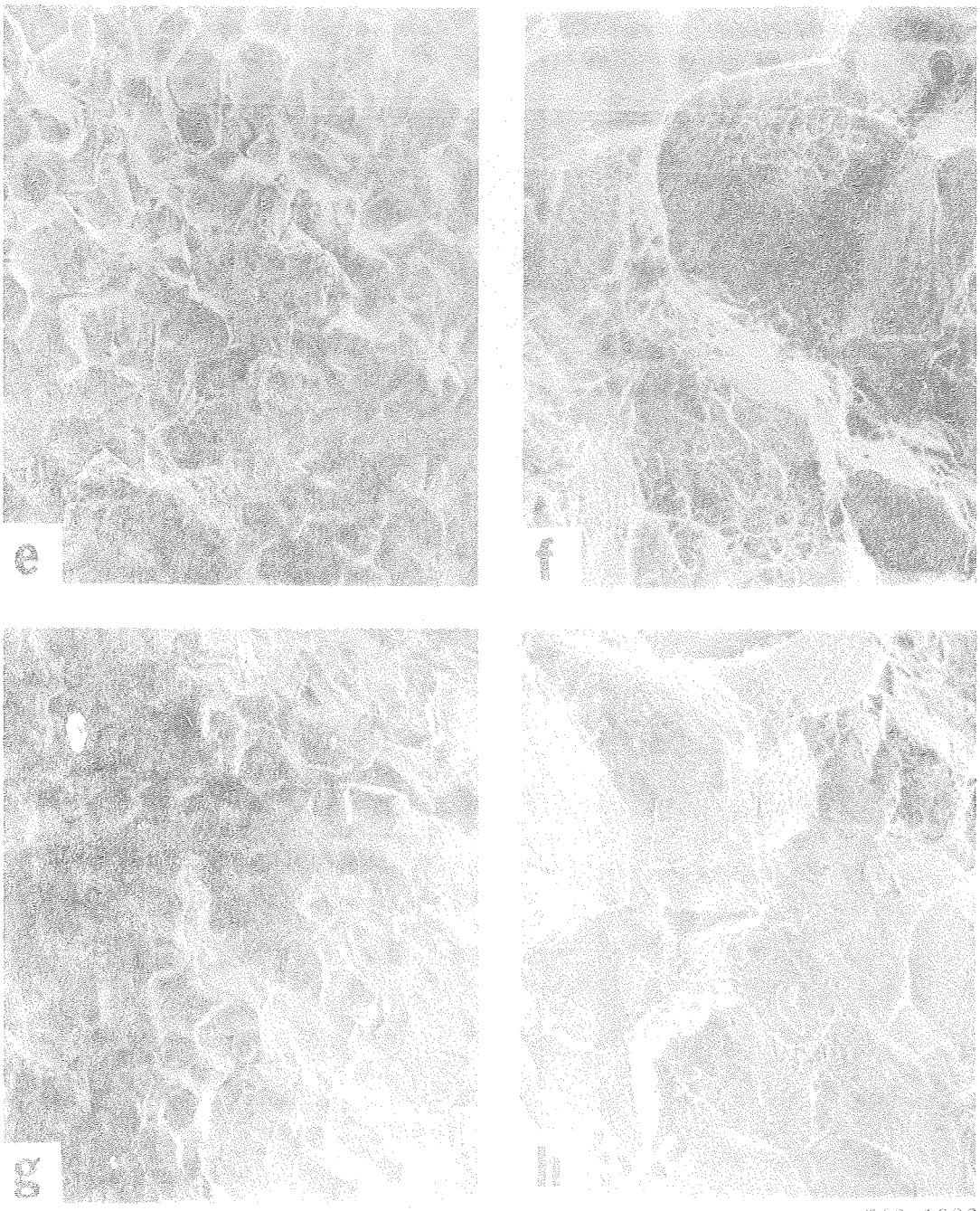

XBB 760-10298

Fig. 8e-h

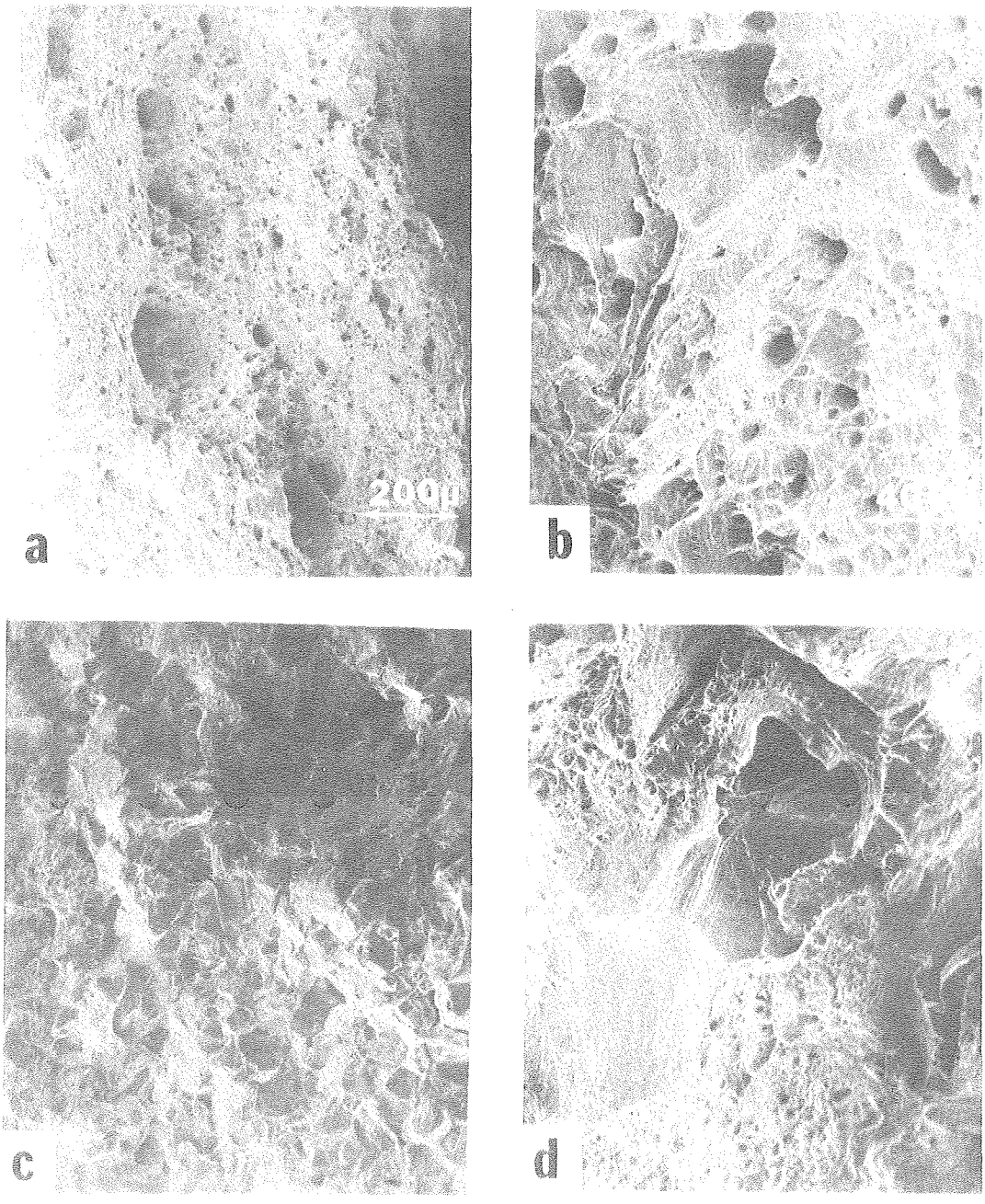

XBB 760-10299

Fig. 9a-d

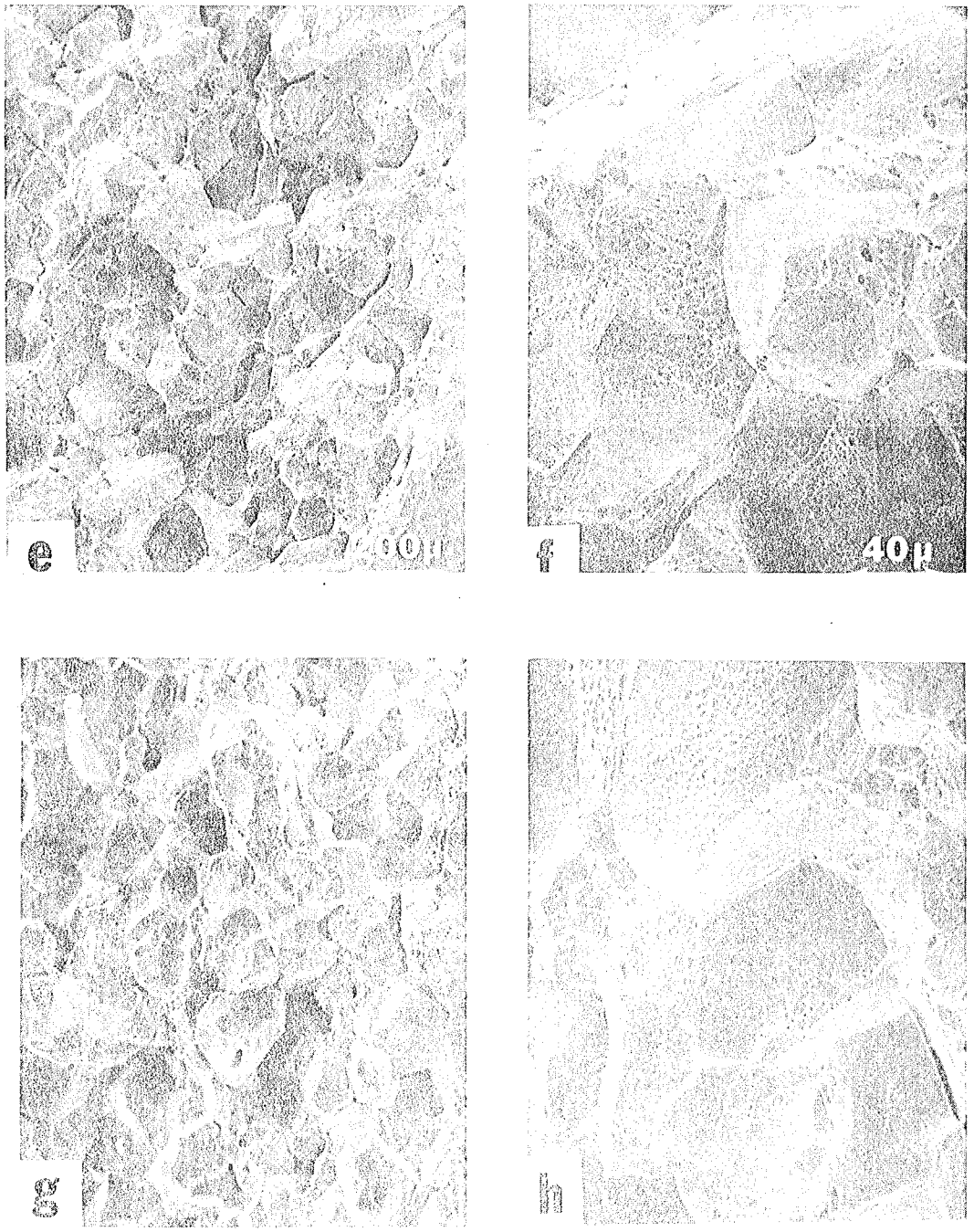

XBB 760-10302

Fig. 9e-h

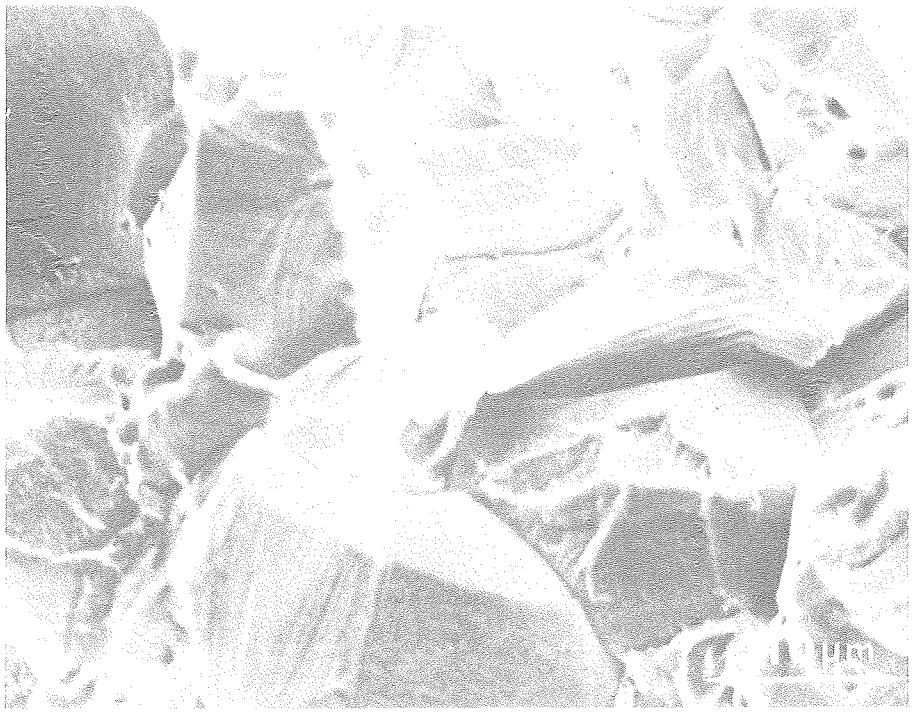

XBB 760-10300

Fig. 10

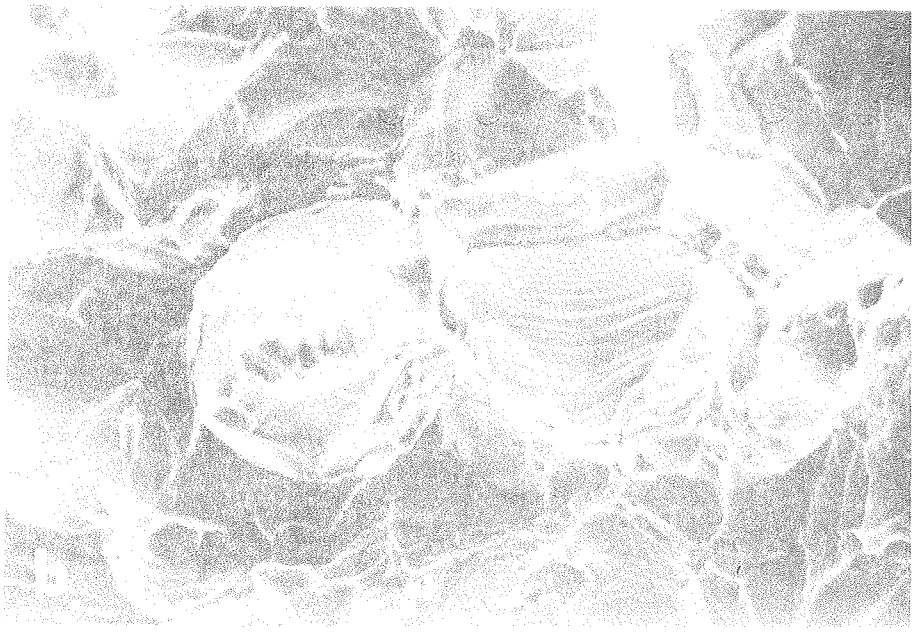

XBB 760-10301

Fig. 11

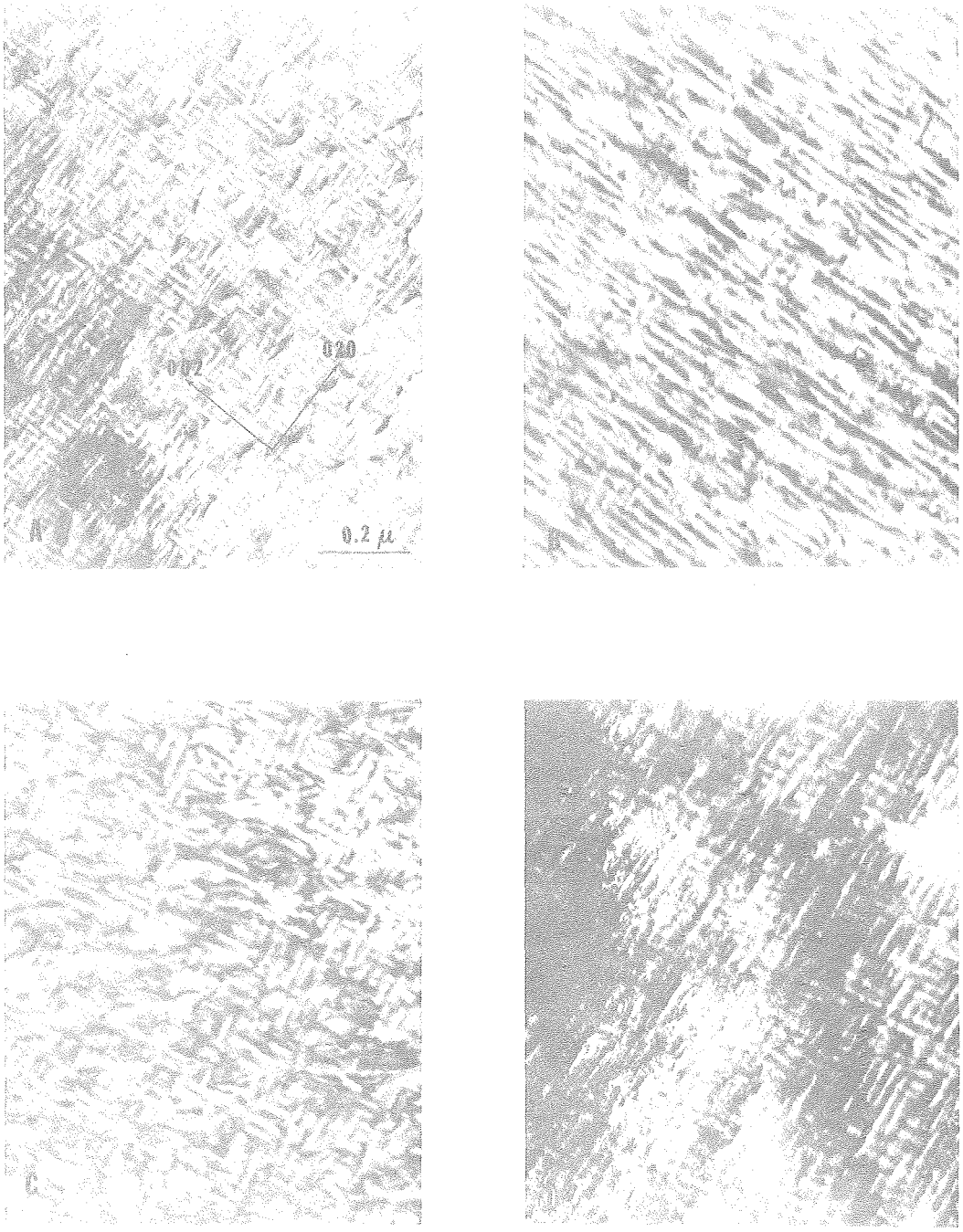

Fig. 12

XBB 769-8353

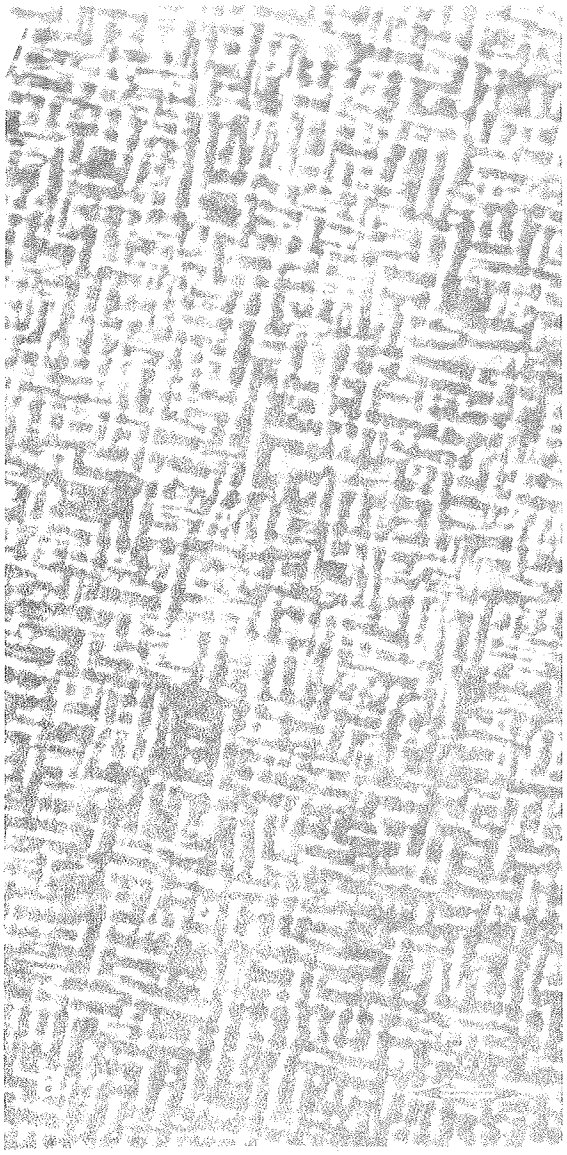

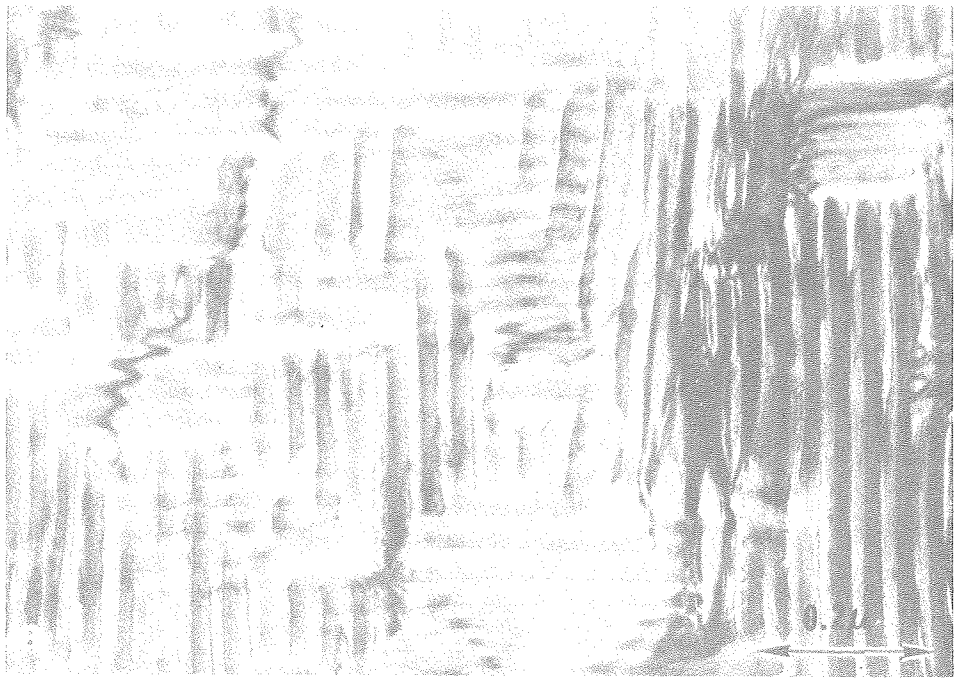

XBB 760-10909

Fig. 14

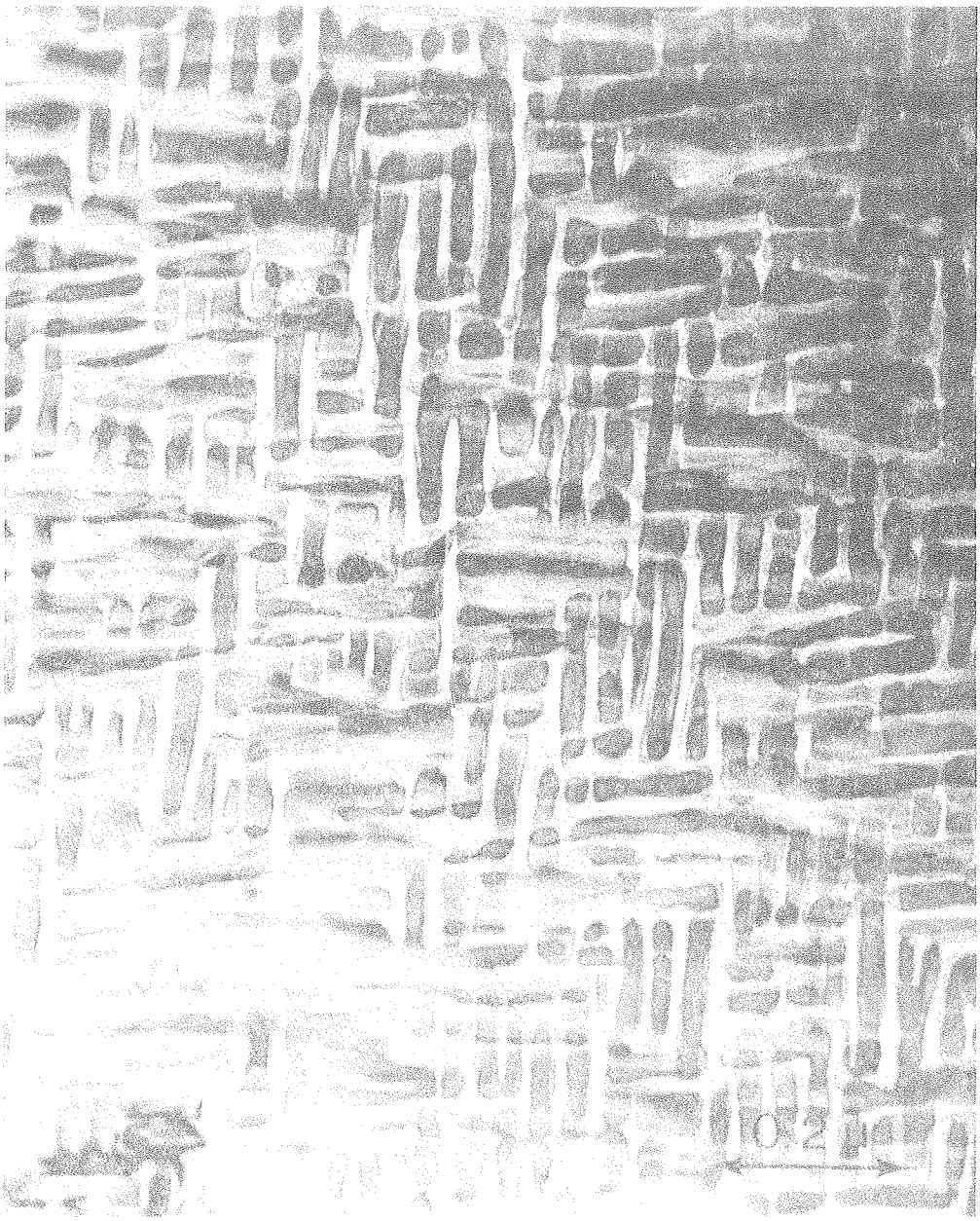

Fig. 15

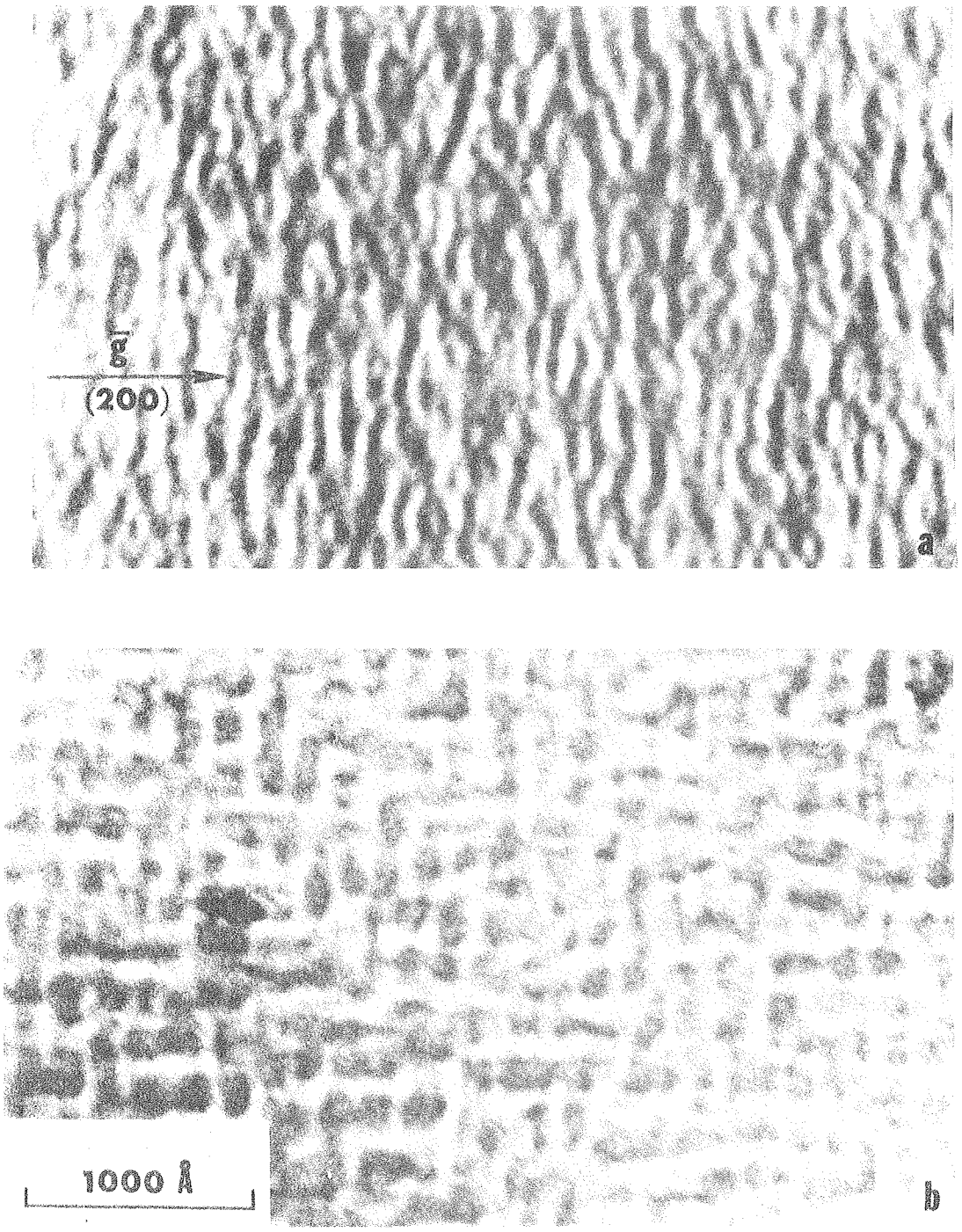

XBB 708-3703

Fig. 16

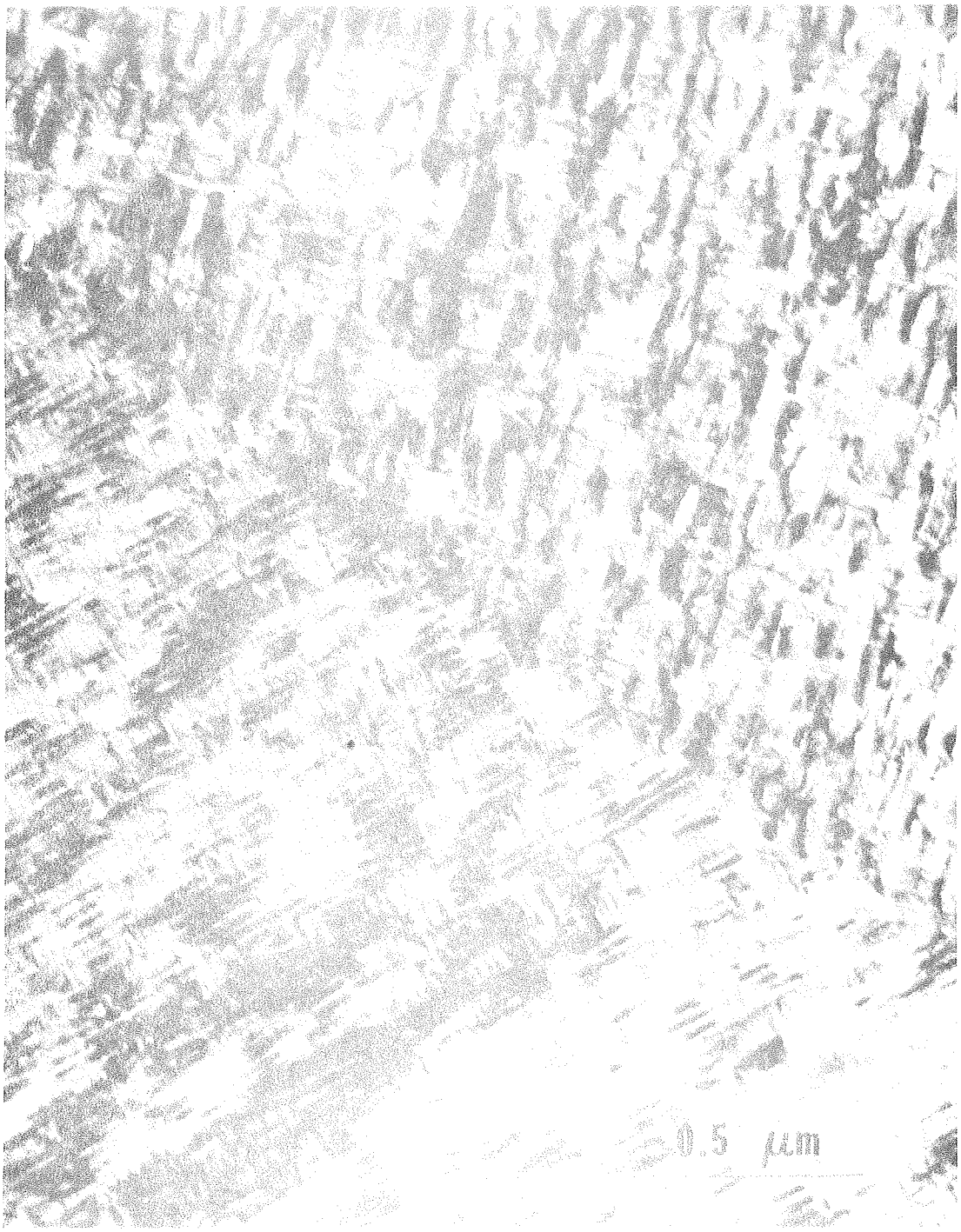

Fig. 17

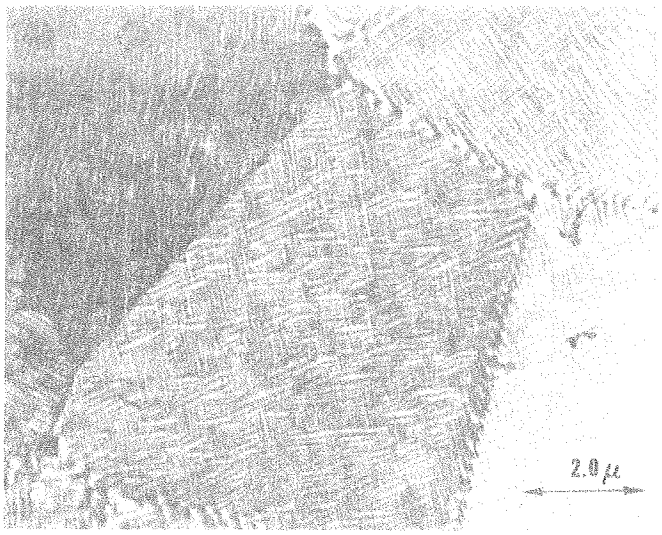

Fig. 18

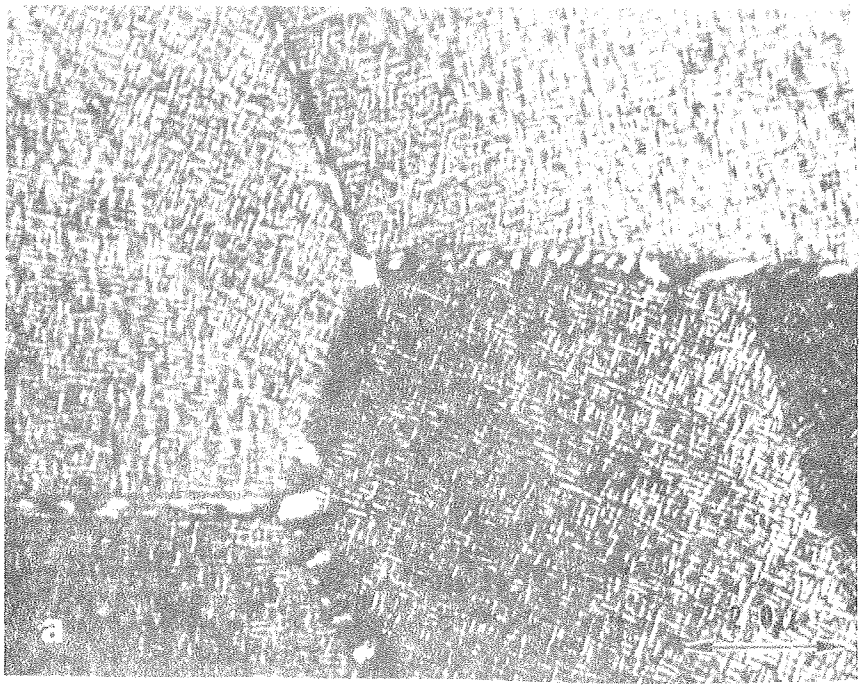

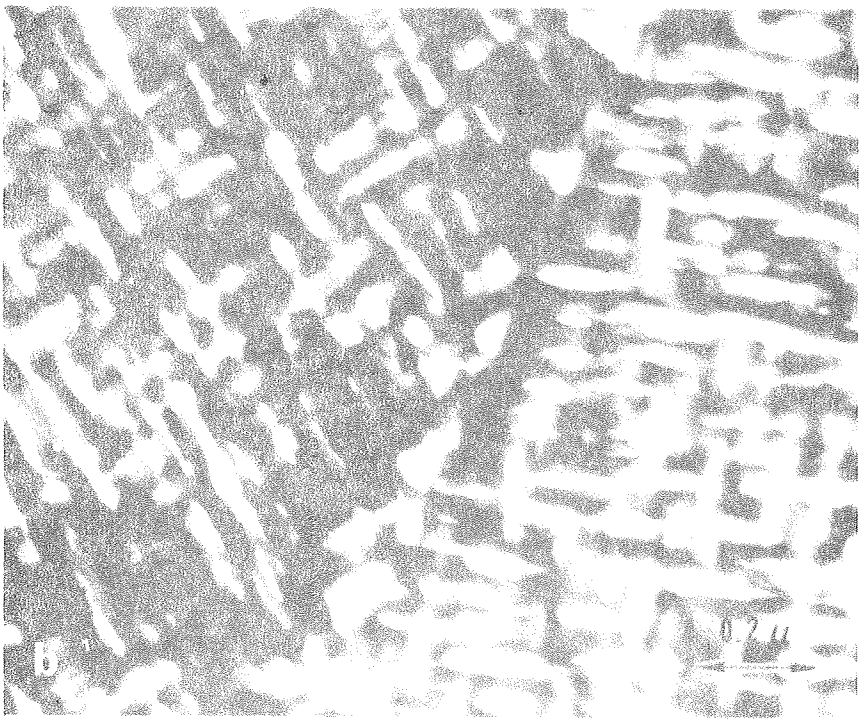

XBB 760-10907

Fig. 19

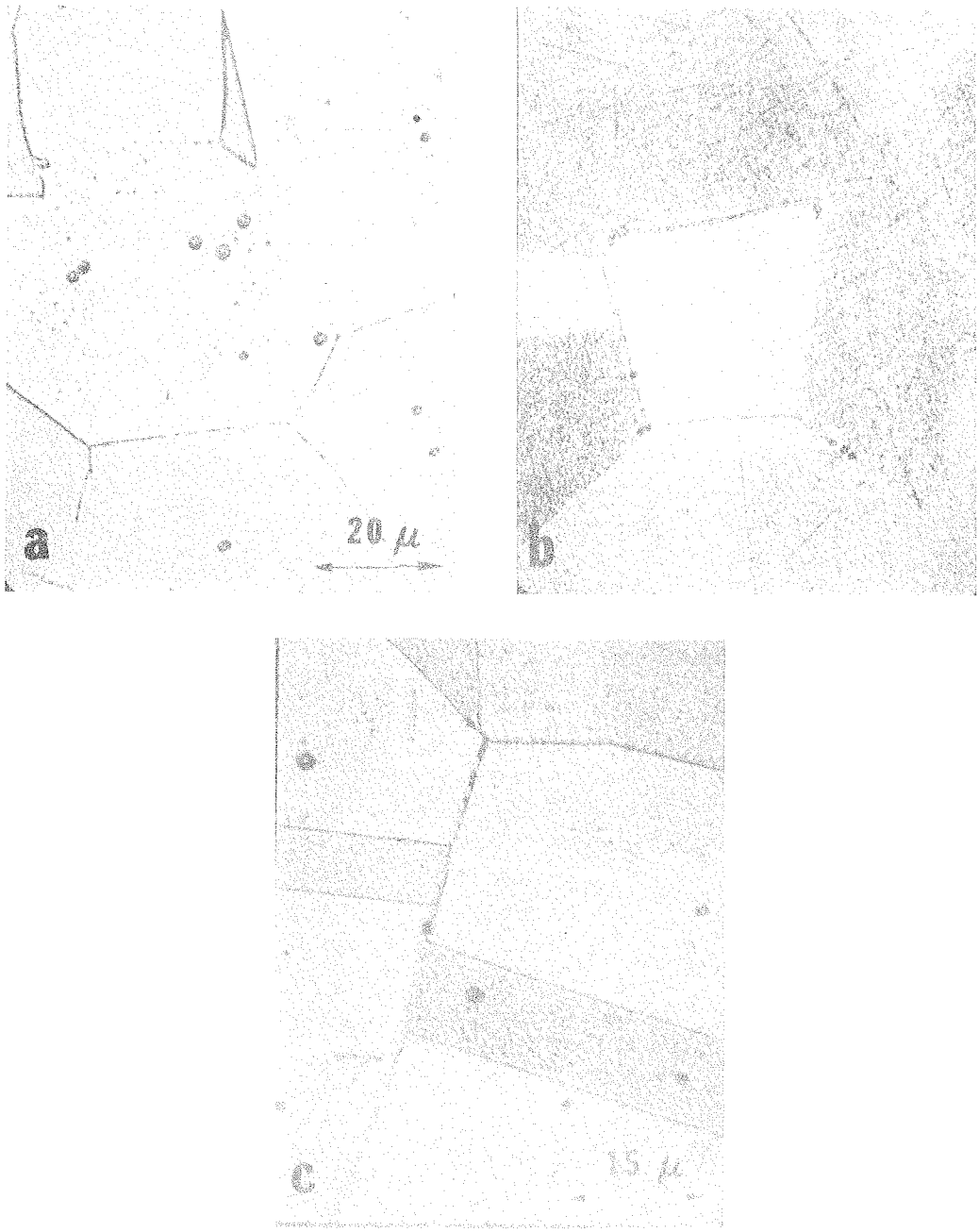

XBB 760-10305

Fig. 20

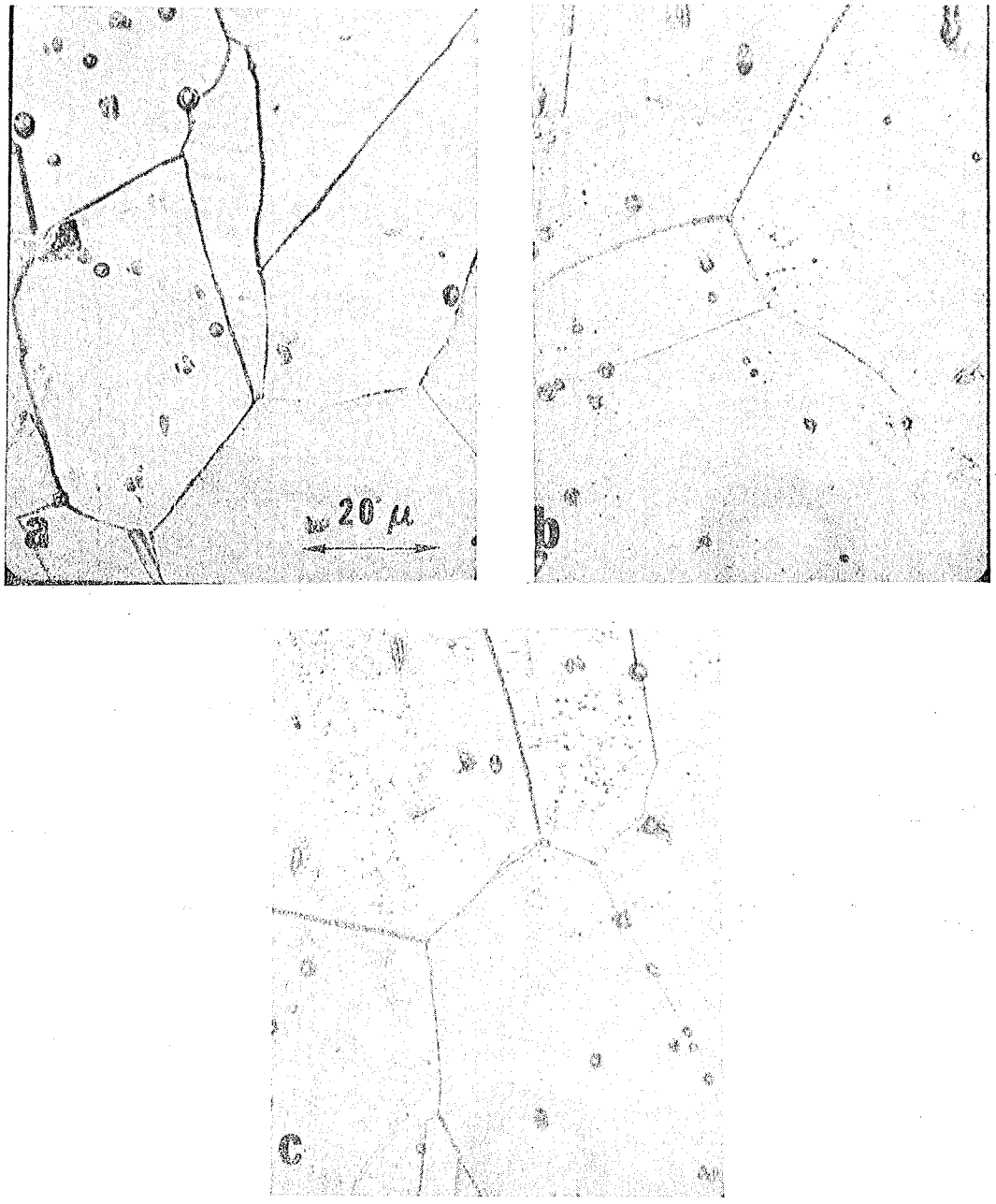

XBB 760-10304

Fig. 21

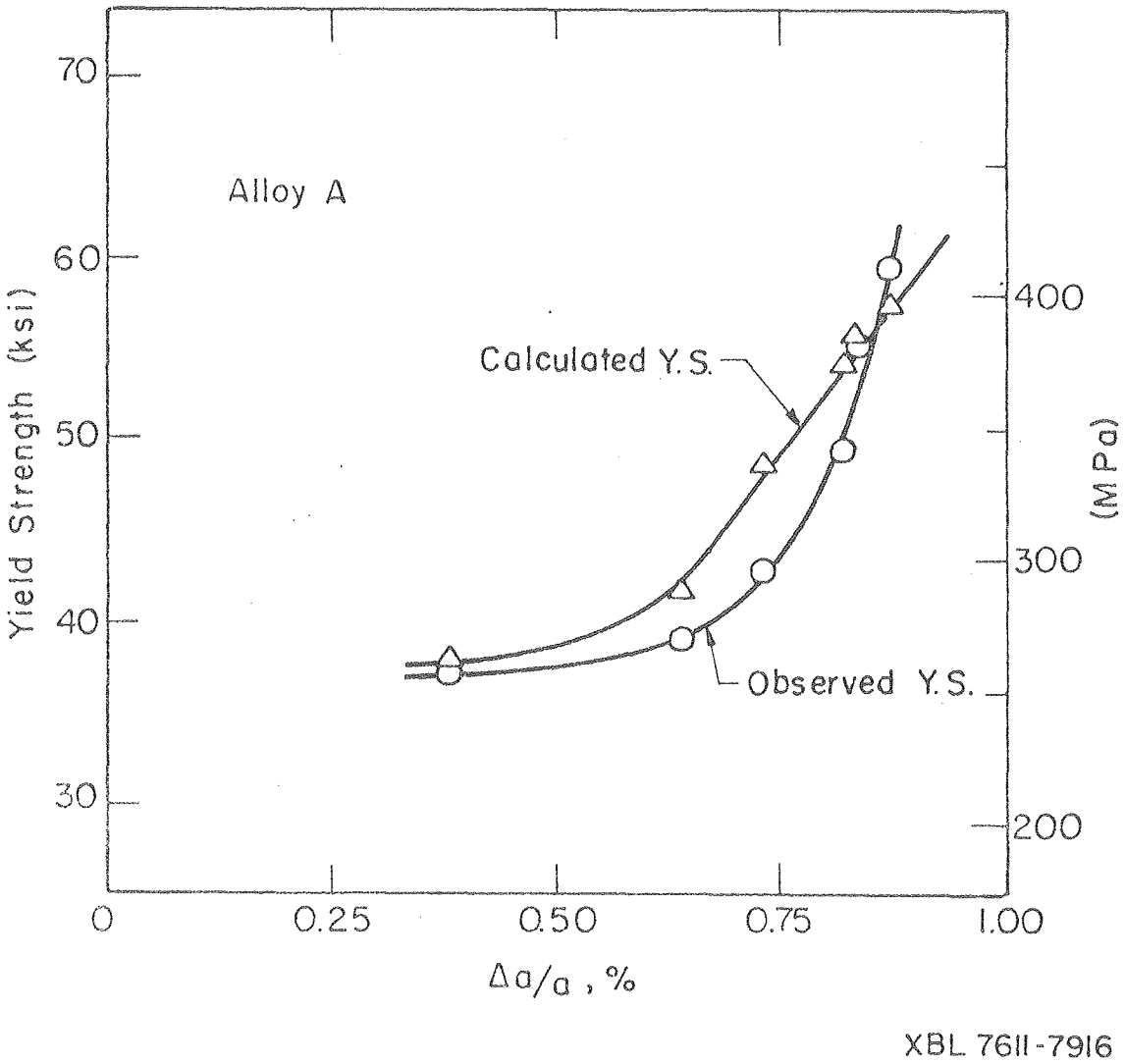
Alloy A
Calculated Y.S.
Observed Y.S.
Yield Strength (ksi)
(MPa)
70
60
50
40
30
400
300
200
0
0.25
0.50
0.75
1.00
Δa/a , %
XBL 7611-7916

Fig. 22

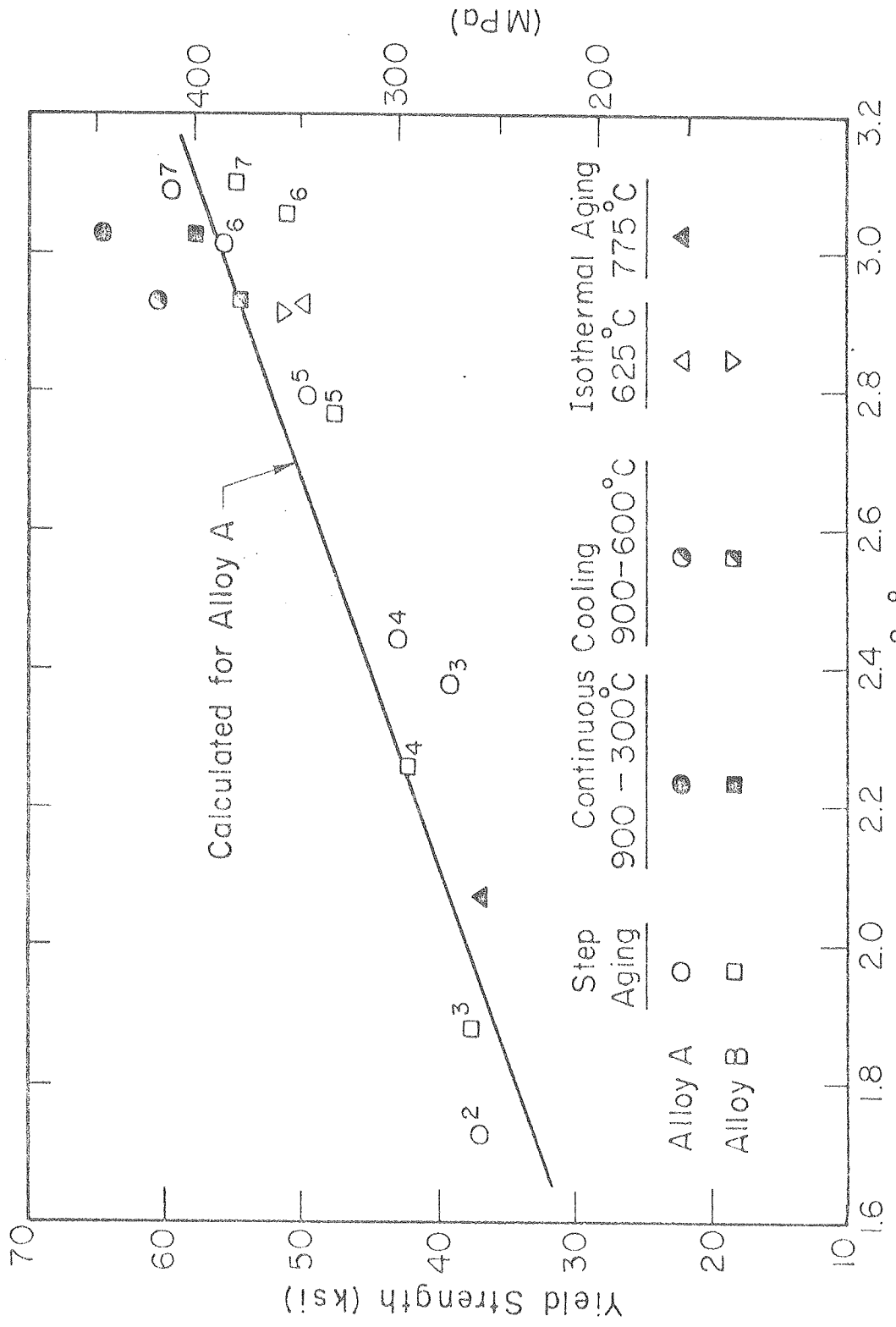

XBL 7611-7917

Fig. 23

This report was done with support from the United States Energy Research and Development Administration. Any conclusions or opinions expressed in this report represent solely those of the author(s) and not necessarily those of The Regents of the University of California, the Lawrence Berkeley Laboratory or the United States Energy Research and Development Administration.